THESIS FOR THE DEGREE OF LICENTIATE OF ENGINEERING

Energy Harvesting and Energy Storage for Wireless and Less-Wired Sensors in Harsh Environments

ELOF KÖHLER

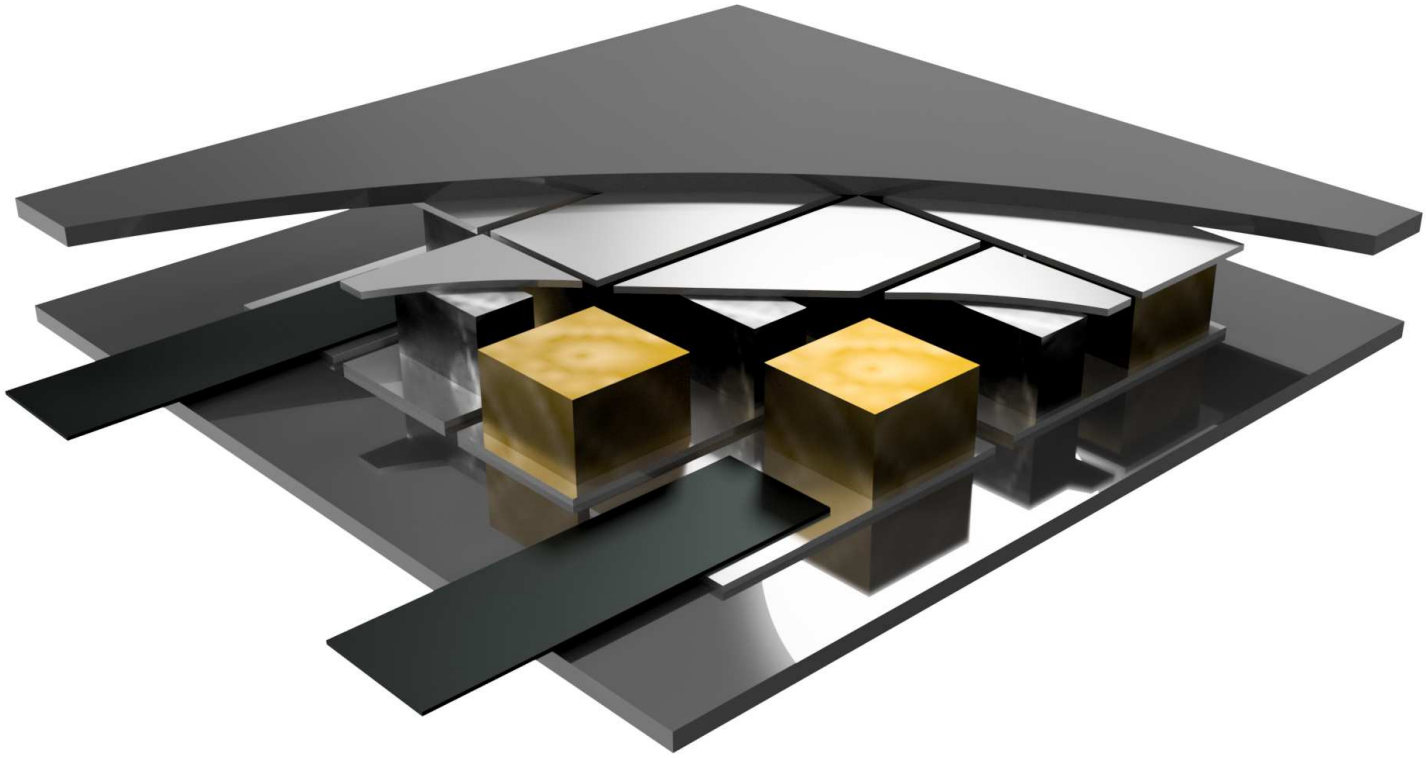

Department of Microtechnology and Nanoscience
CHALMERS UNIVERSITY OF TECHNOLOGY
Gothenburg, Sweden, 2018

Energy Harvesting and Energy Storage for Wireless and Less-Wired Sensors in Harsh Environments
ELOF KÖHLER

Micro and Nanosystems Group
Electronic Materials and Systems Laboratory
Department of Microtechnology and Nanoscience
Chalmers University of Technology
SE–412 96 Gothenburg
Sweden
Telephone +46 (0)31–772 1000

Printed by Chalmers Reproservice
Gothenburg, Sweden, 2018

Det finns inga dåliga väder, bara dåliga skor.

Energy Harvesting and Energy Storage for Wireless and Less-Wired Sensors in Harsh Environments
ELOF KÖHLER
Department of Microtechnology and Nanoscience
Chalmers University of Technology

Abstract

Engineering requires sensors to control and understand the environment. This is particularly important in harsh environments. The drawbacks, especially in gas turbines is the complexity of installing a wired sensor and the weight of the wires. This makes wireless sensors attractive.

A wireless sensor requires a power source for transmission of data. Batteries have previously taken the role of power source for most wireless sensors, but is unfortunately not suitable for all applications. Lately, with energy harvesting and supercapacitors in the picture, sensor applications in high temperature environments, with high power requirements or with long life requirements have the possibility of wireless interface.

A supercapacitor can handle higher temperatures, higher power output and can have a cycle life that exceeds batteries by a factor of 10000. The lower energy density and high self-discharge makes it unsuitable to power a wireless sensor without power source. However, connected to an energy harvester converting waste energy into electricity makes this a powerful combination.

Energy harvesters thrives in environments where waste energy is plentiful and low conversion efficiencies can be enough to power both the sensor and the transmitter. A thermoelectric harvester is designed and fabricated for the middle to rear part of a gas turbine. The temperature in this region can reach 1600°C and require extensive cooling. In the cooling channels the wall temperature reach 800-950°C when the cooling air is 450-600°C. In this location a thermoelectric harvester will have access to high thermal gradients and active cooling.

To harvest the vibrations a piezoelectric energy harvester was built. To harvest enough energy the resonance frequency of the energy harvester is frequency-matched with the high energy vibrations. In many applications these frequencies drift and thus require a broad bandwidth harvester. Simulation and assembly of a broadband coupled piezoelectric energy harvester is presented in the thesis.

A piezoelectric harvester require electronics and energy storage to gather enough energy to power up and run a wireless sensor. The thesis covers the fabrication of a high temperature supercapacitor capable of temperatures up to 181°C.

Keywords: Energy harvester, supercapacitor, harsh environment, Thermoelectric, Piezoelectric, Thermoelectric harvester, piezoelectric harvester, coupled harvester

Acknowledgments

I would like to thank the following people:

My deep gratitude to my supervisor and examiner Peter Enoksson for all the support, guidance, discussions and inspiration.

My co-supervisor Anders Palmqvist for your support and knowledge.

Henrik Staaf for the scientific collaborations, the discussions about everything and the fun during both travel and work.

Richard Heijl for all your help with the thermoelectric materials.

Per Lundgren for making teaching something I enjoy and want to improve in.

Sofia, Volodomyr, Mazharul, Amin, Markus and Qi for the scientific collaborations and the nice atmosphere at work.

Sanel Zenkic, Anders Lindblom and Edvard Svenman at GKN Aerospace for nice collaboration and help with measurements

Patric and Mattias for all the awesome coffee breaks.

Elof Köhler
Gothenburg, Sweden
January, 2018

List of Publications

Paper I

High Temperature Energy Harvester for Wireless Sensors

E. Köhler, R. Heijl, L.G.H. Staaf, S. Zenkic, E. Svenman, A. Lindblom, A. Palmqvist and P. Enoksson

In *Smart Materials and Structures*,
vol. 23, 095042, 2014.

Paper II

Analytic modeling of a high temperature thermoelectric module for wireless sensors

E. Köhler, L.G.H Staaf, A. Palmqvist and P. Enoksson

In *Journal of Physics: Conference Series 557*,
Vol. 557, 012085, 2014

Paper III

Simulation and Experimental Demonstration of Improved Efficiency in Coupled Piezoelectric Cantilevers by Extended Strain Distribution

L.G.H. Staaf, E. Köhler, D. Parthasarathy, P. Lundgren and P. Enoksson

In *Sensors and Actuators A: Physical*,
Vol. 229, p. 136-140, 2015

Paper IV

Supercapacitor with increased capacitance at 200°C

E. Köhler, L.G.H. Staaf and P. Enoksson

In *IET Conference Publications. EVI-GTI and PIWG Joint Conference on Gas Turbine Instrumentation*,
CP693, 2016

Contributions

Paper I

Responsible for design, analytic modeling, simulations, assembly, measurements on module and partly synthesis. Wrote manuscipt, except synthesis.

Paper II

Responsible for all parts.

Paper III

Partly responsible for building device, simulation strategies, measurement setup and measurements. Partly responsible for ideas and partly responsible for writing conclusion.

Paper IV

Responsible for measurement setup and measurements. Partly responsible for idea and building supercapacitor. Responsible for writing and presenting work.

Other publications

Fabrication of High Temperature Thermoelectric Energy Harvesters for Wireless Sensors

E. Köhler, R. Heijl, L.G.H. Staaf, S. Zenkic, E. Svenman, A. Palmqvist and P. Enoksson

In *13th International Conference on Micro and Nanotechnology for Power Generation and Energy Conversion Applications (PowerMEMS2013)*,
Vol. 476, 012036, (2013)

Modelling and experimental verification of more efficient power harvesting by coupled piezoelectric cantilevers

L.G.H. Staaf, E. Köhler, D. Parthasarathy, P. Lundgren and P. Enoksson

In *14th International Conference on Micro and Nanotechnology for Power Generation and Energy Conversion Applications (PowerMEMS2014)*,
Vol. 557, 012098, (2014)

Simulation of a Novel Bridge MEMS-PZT Energy Harvester for Tire Pressure System

L.G.H. Staaf, E. Köhler, D. Parthasarathy, P. Lundgren and P. Enoksson

In *14th International Conference on Micro and Nanotechnology for Power Generation and Energy Conversion Applications (PowerMEMS2014)*,
Vol. 557, 012041, (2014)

Smart design selftuning piezoelectric energy harvester intended for gas turbines

L.G.H. Staaf, E. Köhler, M. Soeiro, P. Lundgren and P. Enoksson

In *15th International Conference on Micro and Nanotechnology for Power Generation and Energy Conversion Applications (PowerMEMS2015)*,
Vol. 660, 012125, (2015)

MEMS Based Micro Aerial Vehicles

N. Joshi, E. Köhler and P. Enoksson

In *27th Micromechanics and Microsystems Europe Workshop*,
Vol. 757, 012035, (2016)

Evaluation of 3D printed materials used to print WR10 horn antennas

E. Köhler, S. Rahiminejad and P. Enoksson

In *27th Micromechanics and Microsystems Europe Workshop*,
Vol. 757, 012026, (2016)

Direct 3D printed shadow mask on Silicon

S. Rahiminejad, E. Köhler and P. Enoksson

In *27th Micromechanics and Microsystems Europe Workshop*,
Vol. 757, 012021, (2016)

Piezoelectric energy harvesting as energy source for autonomous intelligent wireless systems on gas turbines

L.G.H. Staaf, E. Köhler, J. Kemp, M. Allen, S. Zenkic, A. Lindblom, M. Christodoulou and P. Enoksson

In *IET Conference Publications. EVI-GTI and PIWG Joint Conference on Gas Turbine Instrumentation*,
CP693 (2016)

Miniaturized Supercapacitors for Smart Systems

Q. Li, V. Kuzmenko, M. Hague, P. Lundgren, E. Köhler, L.G.H Staaf and P. Enoksson

In *Smart Systems Integeration 2017*,
Cork, Ireland (2017)

Rapid manufacturing of OSTE polymer RF-MEMS components

S. Rahiminejad, J. Hansson, E. Köhler, W. Winjngaart, T. Haraldsson, H. Sjoerd and P. Enoksson

In *Proceedings of the IEEE International Conference on Micro Electro Mechanical Systems (MEMS)*,
p. 901-904. (2017)

Nanocomposite materials for miniaturized supercapacitors

Q. Li, V. Kuzmenko, M. Hague, P. Lundgren, E. Köhler, L.G.H Staaf and P. Enoksson

In *International Conference and Exhibition on Integration Issues of Miniaturized Systems 2017*,
p. 199-205. (2017)

Smart design piezoelectric energy harvester with self-Tuning

L.G.H Staaf, E. Köhler, P. Folkow and P. Enoksson

In *Journal of Physics: Conference Series. 28th Micromechanics and Microsystems Europe Workshop, MME 2017*,
Vol. 922, 012007, (2017)

Selftuning energy harvester by sliding weight

L.G.H Staaf, E. Köhler, P. Folkow and P. Enoksson

In *Svenska Mekanikdagarna 2017*,
(2017)

Verification of self-tuning 4DOF piezoelectric energy harvester with enhanced bandwidth

L.G.H Staaf, E. Köhler, A. Smith, P. Folkow and P. Enoksson

In *The 17th international conference on Micro and Nanotechnology for Power Generation and Energy Conservation Application (PowerMEMS2017)*,
(2017)

Thermal Influence on the Electrochemical behavior of a supercapacitor containing an ionic liquid electrolyte

M. Hague, Q. Li, A. D. Smith, V. Kuzmenko, E. Köhler, P. Lundgren and P. Enoksson

In *Electrochimica Acta*,
(2018)

Achieving increased bandwidth for 4 degrees of freedom self-tuning energy harvester

L.G.H. Staaf, A. D. Smith, E. Köhler, P. Lundgren, P. Folkow and P. Enoksson

In *Journal of Sound and Vibration*,
(2018)

List of Acronyms

TEG	Thermoelectric Generator
RTG	Radioisotope Thermoelectric Generators
zT	Figure of Merit for thermoelectric material
ZT	Figure of Merit for thermoelectric device
PZT	Lead Zirconate Titanate
RMS	Root Mean Square
PTFE	Polytetrafluoroethylene
NASA	National Aeronautics and Space Administration
EMIM Ac	1-Ethyl-3-methylimidazolium acetate
STARGATE	Sensors Towards Advanced Monitoring and Control of Gas Turbine Engines

Contents

CHAPTER 1

Introduction

There is a constant need to measure the environment. To measure the outdoor temperature, to evaluate if there is someone in the passenger seat in the car or to measure the temperature in a nuclear fuel rod inside a nuclear reactor. The type of environment and application dictates what kind of sensor that should be used but also how this sensor is best powered and how the information is communicated. The sensor need to have an appropriate measurement range and work within a specified accuracy, but also account for power requirement depending on the available power source. This can be especially important when the sensor communication is wireless.

There are different levels of wireless sensing, ranging from sensors powered externally but with wireless communication to neat solutions where power supply, sensor and transmitter are all combined in one package. Sometimes the reality is somewhere in between and a more suitable name would then be less-wired sensors [1].

A wireless sensor require a power source which depends on the application, environment and type of sensor. A battery is often preferred with the combination of high energy content, low self-discharge and low cost. If for some reason the environment is not suitable e.g. the temperature is too high, the sensor is inaccessible under long periods of time or the peak power is too high the battery should be replaced or combined with other power source solutions. An example of a wireless sensor system can be seen in Fig. 1.1 where a thermoelectric energy harvester is connected to a power management circuit. The power management circuit stores the energy inside a supercapacitor until the stored energy exceeds the requirement to start the transceiver and transmit the sensor data.

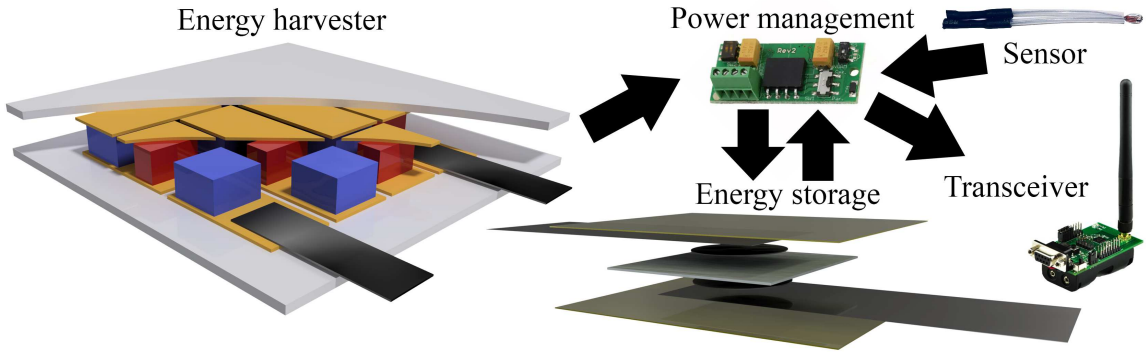

Figure 1.1: An energy harvester converts waste energy to electricity and supplies a power management circuit. If the power exceeds the requirement of the transceiver or if the stored energy is enough the power management delivers power to the transceiver that sends the sensor data.

Supercapacitors can provide higher power outputs than batteries and be charged/discharged with very little degradation, but suffers from higher self-discharge and lower energy content than batteries [2]. Powering a sensor from a supercapacitor alone is not recommended because of the high self-discharge, but a supercapacitor coupled to a battery or an energy harvester can be a powerful combination [3].

The combination of an energy harvester and a supercapacitor is extra powerful in harsh environments where e.g. heat, vibrations or high pressure are plentiful. A supercapacitor can be designed to handle vibrations and high pressures and can even get an energy density boost from operating in high temperatures, as showed in **paper IV**. Energy harvesters thrives in environments where waste energy is plentiful, where low conversion efficiencies can be enough to power the sensor and transmitter, in some cases even without the need of energy storage.

There are many different types of energy harvesters with different properties and challenges that have to be considered. The power output can e.g. be low voltage DC, high voltage AC or pulse based and this can set limits on the resistance in the cables or require additional electronics [4].

Also, with sensor environments where e.g. the temperature is too high for the electronics the sensors cannot be a neat wireless sensor package, instead the electronics have to be on a safe distance from the sensor. Having the energy harvester close to the sensor could be beneficial because of the possible extra energy available in the environment, the possibility to power the sensor with less resistive losses from shorter cables and the use of less cables (weight, cost).

1.1 Background and motivation

One of the key reasons to replacing a wired sensor with a wireless or less-wired sensor is to reduce the amount of wires used, reducing both the cost of the wires and the time needed to install a sensor. Also, even if the wireless sensor can be battery powered there is a wish to have it combined with an energy harvester to increase the life time. To have e.g. a truck that needs to go into service to change sensor batteries is not practical.

In the case of aircraft gas turbines the need for wireless sensors is extended with the wish to reduce weight from the wires. The complexity of both wired and wireless sensors increase in these harsh environments. The biggest obstacles being the very high temperatures and the fact that the sensors are inaccessible. Changing a battery is not possible even if placed at a low temperature location and pulling the cables from the sensors is time-consuming or near impossible at some locations because of the temperature or the moving parts.

A single Rolls-Royce® test gas turbine can contain up to 1500 sensors and 19 km of copper wire [5]. Because of the high temperatures the wire is shielded with MgO and stainless steel which increases weight and cost to a point where it is a problem despite the fact that a test gas turbine never leaves ground.

Parts of the thesis work has been in close collaboration with several other European universities and companies connected to the aerospace industry through the European funded project STARGATE [1], mainly GKN aerospace, Rolls Royce PLC® UK, Coventry University and SCITEK Consultants LTD. Our goal was to find energy harvesting and energy storage solutions to make

it possible to replace some of these sensors by wireless or less-wired sensors. Two different types of energy harvesters has been developed, vibrational and thermal energy harvesters.

The vibrational energy harvester is based on the classified vibrational data available from an ex-service Rolls-Royce® gas turbine and was designed to work during start up and at cruise speed. The vibrational data showed that a broad bandwidth harvester was crucial and a coupled harvester was proposed. This coupled piezoelectric harvester is explained in **paper III** and chapter 3.

Given the information about problematic wired sensor locations and temperatures in the test gas turbine rig a thermal energy harvester was designed to replace wired sensors in the middle to rear of the gas turbine [5]. The air temperature in this regions can reach 1600°C and require active air cooling through cooling channels [6]. The walls in the cooling channels have a more moderate 800-950°C temperature and the high flow cooling air a temperature of around 450-600°C. A thermal energy harvester in this location would have access to both active cooling and a high thermal gradient, ideal for a thermoelectric energy harvester. The design and assembly of such a harvester is explained in **paper I**, **paper II** and chapter 2.

The energy storage development in this thesis is mainly focused on temperatures above 125-150°C where most high temperature batteries have reached their limit [7]. With supercapacitors it is possible to go higher in temperature but there is still challenges to solve. The assembly and measurements on high temperature supercapacitors with liquid electrolyte is discussed in **paper IV** and chapter 4.

1.2 Wireless energy harvester sensor system

Although the main topic of this thesis is the energy harvesting and energy storage, it is inescapable to discuss the complete wireless sensor system, because the design of the harvesters and energy storage need to be matched with the rest of the system. With the goal to power a wireless sensor with energy harvesting, the power requirements from sensor and transmitter are important for the design. The power losses from cables, power electronics and the self-discharge of the supercapacitor need to be accounted for as well.

There are countless different sensors available with different power requirements e.g. the NOx sensor used in trucks require 30 W [8] while a k-type thermocouple require 1 mW [9]. To reduce the power requirement further it is possible to sample in intervals instead of continuously and to transmit the data in intervals. Within the STARGATE-project data compression was developed by Coventry University to reduce the power consumption. The data compression experiments was focused on temperature measurements with ZigBee wireless interface and CC2430 hardware platform [10, 11]. The energy harvesters are developed for this hardware platform and to measure the temperature with a thermocouple.

The power management circuit used with the piezoelectric energy harvesters is MIDE EHE004 [12]. The use of power management circuit is especially important for vibrational harvesters in order to convert the AC output into DC output. The EHE004 can also be combined with a supercapacitor that store the energy and only release power to the transmitter when a certain

voltage is reached in the supercapacitor, 4.04 V or 5.05 V depending on the chosen output voltage. If the voltage drops beneath a certain voltage in the supercapacitor the circuit cuts power to the transmitter and the supercapacitor can charge again. The circuit has four different output voltages to choose between (1.8 V, 2.5 V, 3.3 V and 3.6 V), all of them appropriate with the CC2430.

For the thermal harvester the power management is needed for DC-DC boosting, especially for a thermoelectric energy harvester with only a few thermocouples. To boost a voltage output starting at 20 mV the power management circuit LTC3108 was chosen [13]. At this low voltage the efficiency only reaches around 25-30% when boosting to 3.3 V. Conversion efficiencies as low as 25% add an extra incentive to increase the voltage output from the energy harvester.

1.3 Scope and outline of thesis

Two different types of energy harvesters have been developed, one vibrational energy harvester based on the classified vibrational data acquired from Rolls-Royce PLC® and one thermal energy harvester designed for the cooling channels in the middle to rear of the gas turbine.

Paper I and **paper II** covers the analytical modeling, synthesis, assembly and measurements on the thermoelectric energy harvester designed for this test gas turbine. Because of the complexity of the design of the thermoelectric energy harvester, chapter 2 expands on **paper I** and **paper II** to get a more detailed picture of the design.

For the vibrational energy harvester, the design and assembly of this coupled harvester was the main contribution, most of the parts were off-the-shelf. Chapter 3 describes the coupled piezoelectric harvester and in **paper III** the simulation and experimental validation of a coupled piezoelectric energy harvester is demonstrated.

With the cooling air reaching temperatures above 450°C there are no available options for electronics. No wireless transmitter or AC-DC/DC-DC converters can survive this temperature. To make a completely wireless sensor this needs to be solved and is out of scope for this thesis. However, for a less-wired sensor the possibility to combine the thermal harvester with a high temperature supercapacitor cannot be overlooked.

The exploration of high temperature energy storage is covered in **paper IV** examining the thermal effect on a packaged supercapacitor up to 250°C.

CHAPTER 2

Thermoelectric Harvester

2.1 Introduction

Even though the thermoelectric effect was discovered in 1820 [14] the use of thermoelectric energy conversion has been limited to very few applications due to the low efficiency, but in recent years new materials have placed thermoelectric generators in the spotlight with efficiencies around 13-15% at 1000 °C and theoretical efficiencies up to 25% [15]. Because thermoelectric generators are solid state they can be made very small and still keep most of the efficiency, under relatively small temperature gradients [16].

Most off-the-shelf available thermoelectric generators have a maximum operating temperature below 325 °C [17] with a few generators operating at higher temperatures up to 800 °C [18]. At temperatures above 800 °C there are no off-the-shelf generators available and to keep high efficiency several thermoelectric materials in segments are needed, making the generators much more complex [19]. These are mainly used in RTGs (radioisotope thermoelectric generators) in NASAs space missions or remote lighthouses [20, 21].

In the middle and rear part of a gas turbine the temperature increases to far above 800 °C and cooling air is pumped through the walls and even the turbine blades to decrease the surface temperature. A thermoelectric energy harvester inside a gas turbine can be placed in one of these cooling channels. In the middle of a gas turbine the sensor cables are the longest and most difficult to place, replacing these with wireless sensors or less wired sensors is highly desirable. At this location the surface temperature is around 800-950 °C and the cooling air 450-600 °C, potentially giving a harvester temperature gradient of over 200 °C over 1 mm. Because the conversion efficiency (zT) of thermoelectric materials are temperature dependent and an application in this area would operate in the unusual temperature span of 600-800 °C an analytical model was made to assess what materials are most suitable. The model was also needed to determine a number of design parameters discussed in Chapter 2.

To convert as much of the available heat as possible, thermoelectric harvesters are typically designed to operate at maximum efficiency. In this application with the excessive amounts of waste energy available, it is instead beneficial to design the thermoelectric harvester to operate at maximum power output. With the challenges of material degradation at temperatures as high as 800°C the design has to include this as well.

2.2 Theory

2.2.1 Seebeck effect

The Seebeck effect is one of the three thermoelectric effects and explains the heat-to-energy conversion. The Seebeck effect is observed when two dissimilar materials are connected and exposed to a thermal gradient. The result is an electrical potential proportional to the temperature difference which is both temperature- and material dependent, called the Seebeck coefficient (V K^{-1}) [22]. There are n-type and p-type thermoelectric materials, with a negative Seebeck coefficient from excess of n-type charge carriers and a positive Seebeck coefficient from excess of p-type charge carriers [23].

2.2.2 Figure of merit

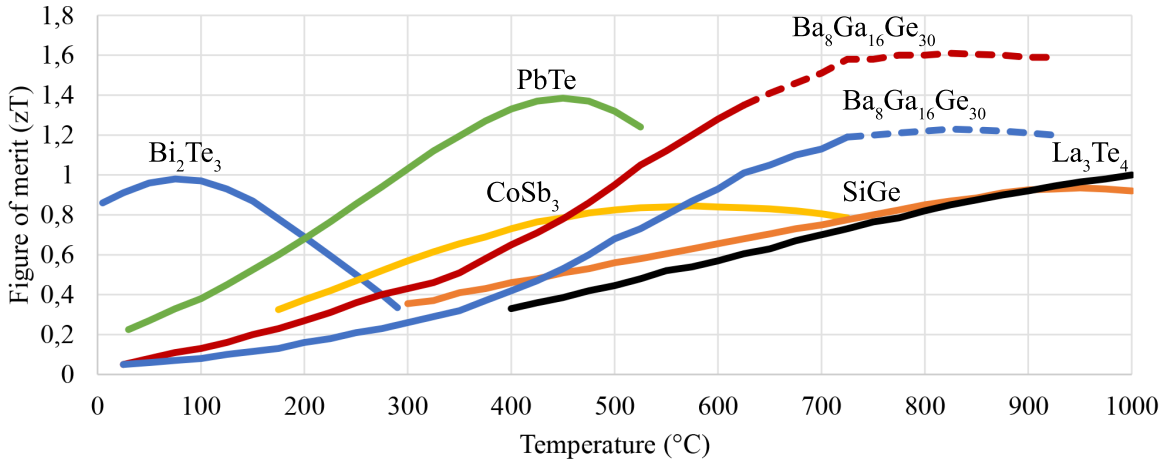

Figure 2.1: zT-value for some common n-type materials between 0-1000°C [23, 24].

The dimensionless "figure of merit" for a material is defined as $zT = \frac{\sigma S^2 T}{\kappa}$, where S is the Seebeck coefficient, σ the electrical conductivity, κ the thermal conductivity and T the temperature. The zT-value is proportional to the efficiency of the material with a theoretical maximum value, the Carnot cycle efficiency [26], at $zT = \infty$. Unfortunately the figure of merit is difficult to increase and improving one attribute usually have negative effect on the others [23], furthermore the zT-value is temperature dependent and has an optimal temperature range where the zT is highest, see Fig. 2.1 and 2.2. For a thermoelectric generator the figure of merit is denoted by ZT.

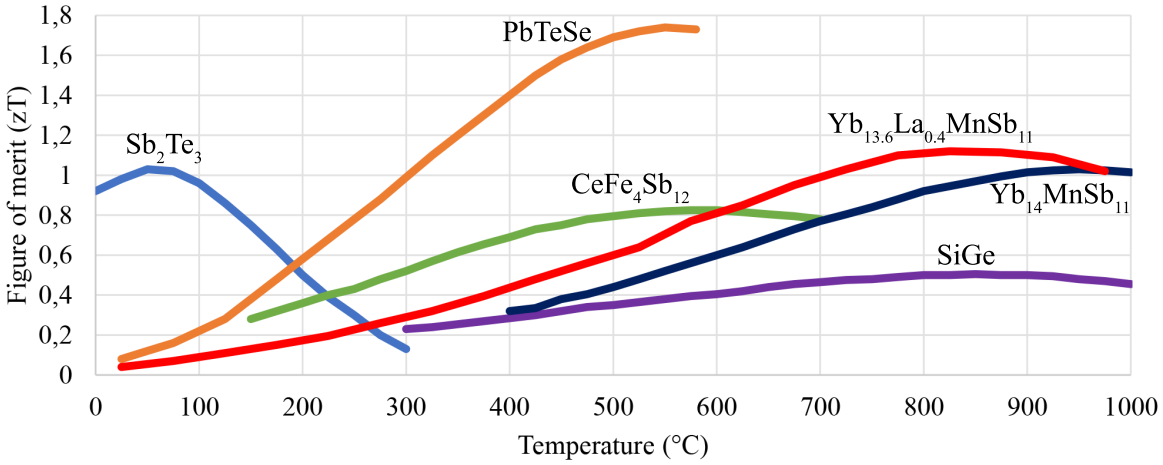

Figure 2.2: zT-value for some common p-type materials between 0-1000°C [23, 25].

2.2.3 Thermoelectric generator

Connecting n-type and p-type materials in parallel thermally and in series electrically induces an electrical current when exposed to a thermal gradient, see Fig. 2.3. This combined "couple" produces a potential in the range of tens to hundreds of μV K^{-1}.

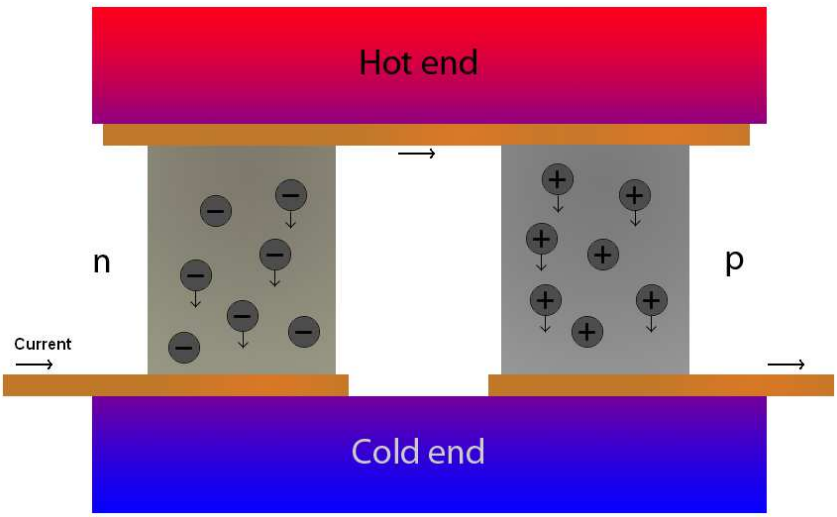

Figure 2.3: Two thermoelectric materials in parallel thermally and in series electrically, current going from left to right and heat from top to bottom.

A thermoelectric generator usually consists of several thermocouples in series to increase the voltage of the device, where each couple consists of one n-type and one p-type leg, see Fig. 2.4. The legs are connected by electrodes placed on electrically insulating and thermally conductive material. High thermal conductivity is important for these to ensure that enough heat are transferred to and from the thermoelectric legs to maintain a high thermal gradient.

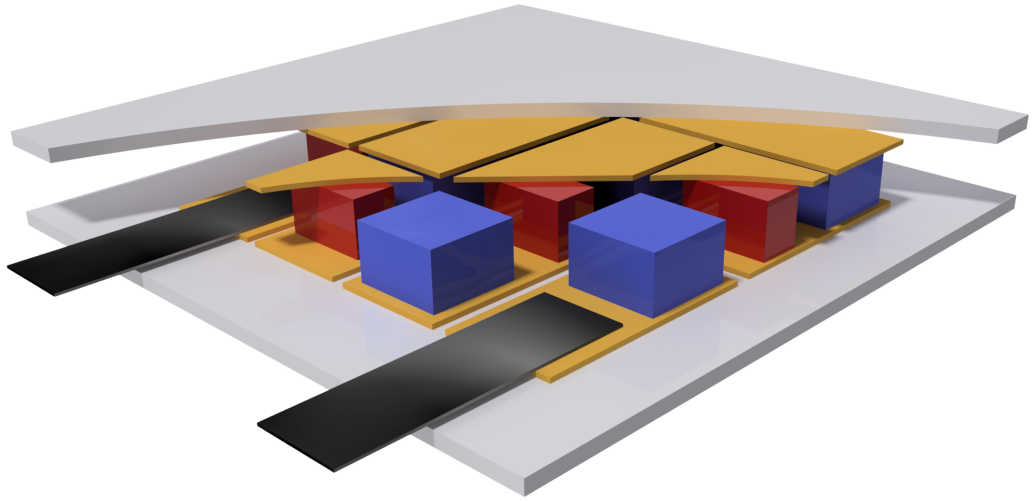

Figure 2.4: Cross section of a thermoelectric device consisting of seven couples between two isolating plates, the two different materials have different size. A second type of electrode are welded to the electrodes inside the device.

When designing a thermoelectric harvester many aspects need to be considered. Not only should the materials have high zT value in the active temperature range but preferably also have similar thermal expansion, electrical- and thermal conductivity and absolute value of the Seebeck coefficient. However, when building harvesters that operate at temperatures above 600°C the number of available materials are substantially reduced.

2.2.4 Power and efficiency

To approximate the power output and efficiency of the thermoelectric generator an analytical model was made. The high thermal gradient, high cold side temperature and the aim to maximize specific power output (W kg^{-1}) makes the application unique and several known analytical models had to be combined to achieve a good analytical model. The derivation of power output is explained in **paper II** and resulted in a power output

$$P = (nS_{avg}T_{diff})^2 \mu / R(\mu + (1+\delta))^2 \tag{2.1}$$

where n is the amount of couples, S_{avg} the average Seebeck coefficient in the temperature range, T_{diff} the temperature difference between the hot- and cold side of the thermoelectric material, μ the load resistance ratio and δ the contact resistance. For the calculation of power output the temperature dependent Seebeck coefficient data for each material is used instead of the average Seebeck coefficient. The electrical and thermal resistance for each material are also included the temperature dependence in the calculations.

2.3 Model

For this particular gas turbine application [1] the weight and size of the device was decided to be approximately 0.5-1 grams and 1-2 cm^2. Because of the size constraint all the materials are included in the calculations to get an approximation of thickness, weight and an indication of where problems could arise during assembly. The high temperature also affects the material properties such as electrical resistivity and thermal conductivity making it important to include these temperature dependent material properties in the calculations. An example is the alumina used as base plates that have a thermal conductivity of about 7 W $m^{-1}K^{-1}$ at 800°C and 37 W $m^{-1}K^{-1}$ at room temperature [27], see Fig. 2.5 and 2.6.

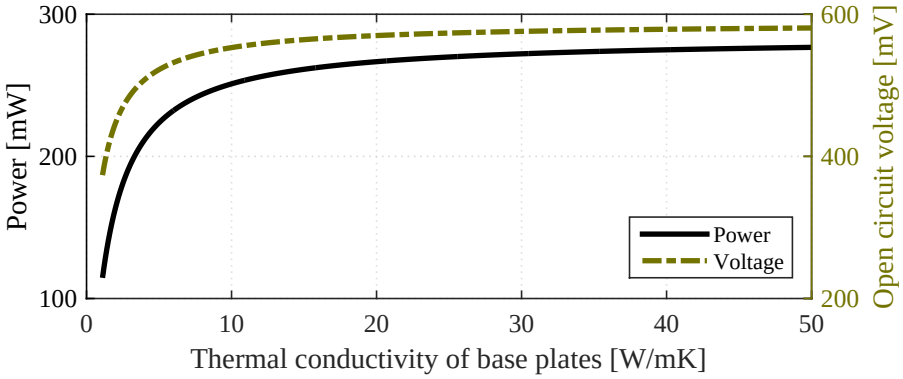

Figure 2.5: The power output and open circuit voltage of a 7-couple device with 1 mm thick base plates as a function of the thermal conductivity of the base plates. Alumina has a thermal conductivity of 7 W $m^{-1}K^{-1}$ at 800°C compared to SiC with 48 W $m^{-1}K^{-1}$. The thermal gradient of the environment is 200°C.

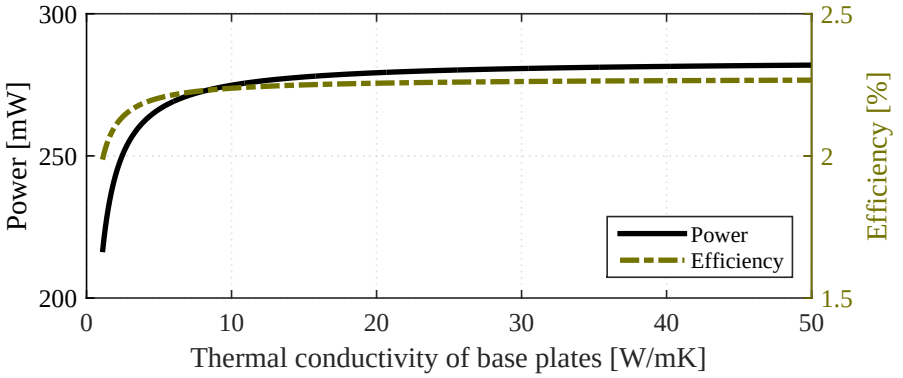

Figure 2.6: The power output and efficiency of a 7-couple harvester with 0.25 mm thick base plates as a function of the thermal conductivity of the base plates. Alumina has a thermal conductivity of 7 W $m^{-1}K^{-1}$ at 800°C compared to SiC with 48 W $m^{-1}K^{-1}$. The thermal gradient of the environment is 200°C.

The calculations was made in Matlab and made it possible to get some first estimations of the heat transfer and power output of the device. Because of the complexity and the number of variables the calculations was done in several steps. Variables included number of couples in square devices (n=1, 3, 7, 11, 17, 23, 31...), height of thermoelectric legs, area of legs, thermal gradient of environment, thermal conductance of base plates, area ratio between n-type and p-type material, thickness of electrodes, electrode resistance, load resistance, parasitic heat conductance between couples, contact resistance and different thermoelectric materials, base plate materials and electrode materials. These variables could then be tuned to find the highest power output possible, including the effect from cables and DC-DC converter, see Fig. 2.7 and 2.8.

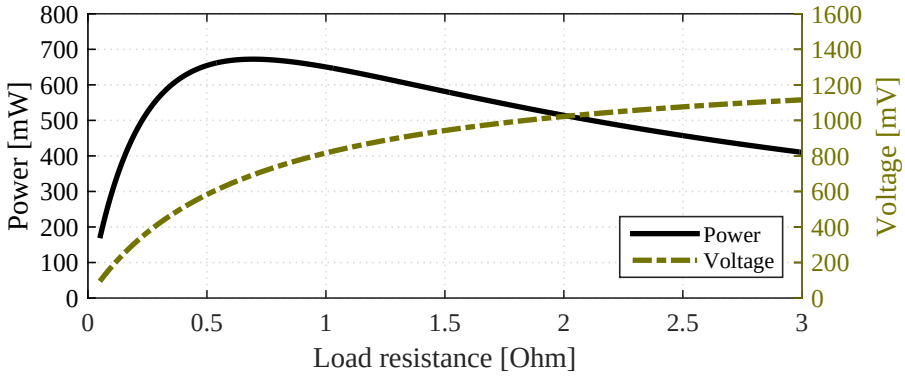

Figure 2.7: The power output and voltage of a 17-couple harvester as a function of the load resistance after losses in cables.

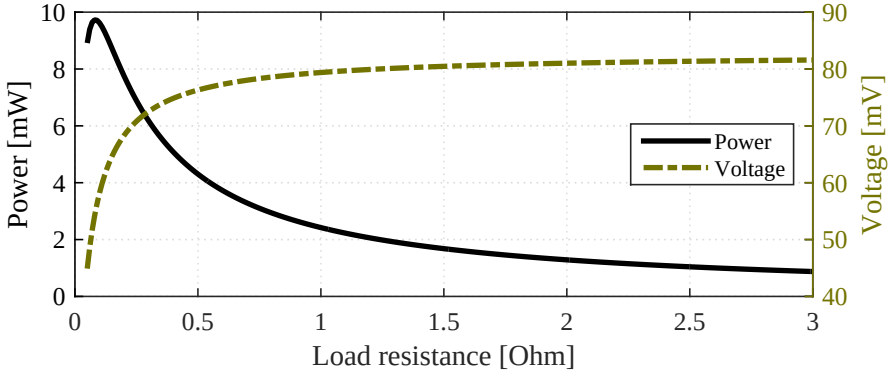

Figure 2.8: The power output and voltage of a 1-couple harvester as a function of the load resistance of the load resistance after losses in cables and DC-DC converter. Because of the low voltage the DC-DC converter efficiency is set to 30%.

The height of the legs have the highest effect on the power output and reducing the leg height means higher power output and lower efficiency, see Fig. 2.9. But shorter legs transfers more heat making it harder to maintain the thermal gradient. A higher thermal gradient on the thermoelectric material also increases stress from thermal expansion and for a 200°C temperature difference the required minimum leg height for a leg with 1.6 mm width is approximately 1 mm

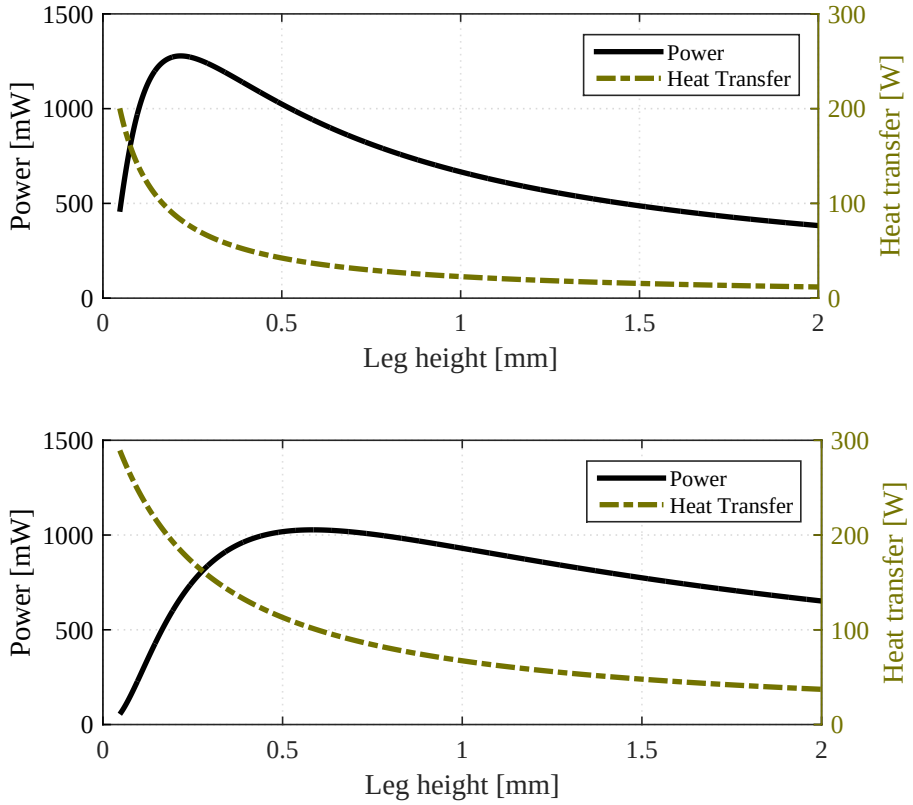

Figure 2.9: Top picture: Power output and heat transfer as a function of leg height for $Ba_8Ga_{16}Ge_{30}$ and $Yb_{14}MnSb_{11}$. Bottom picture: Power output and heat transfer as a function of leg height for SiGe.

[28]. The ability to maintain the thermal gradient depends on the amount of heat available, the heat transfer to the device and the heat transfer through the device. In this project, the amount of heat available is huge and the device is very small, even with very low efficiency the waste is negligible compared to the available energy. To simplify the model the hot- and cold temperatures of the harvester was set as constants because of the high gas flow in the gas turbine. However, to keep the heat sink at a reasonable size the maximum heat input has to be limited according to Eq. 2.2 [29]:

$$P_D = \frac{T_J - T_A}{\theta} \tag{2.2}$$

With a junction temperature (T_J) at 600°C, a cooling air temperature (T_A) around 500°C and a thermal resistance of 4°C W^{-1} gives a power dissipation (P_D) of 25 W. The estimated thermal resistance of 4°C W^{-1} could be achieved with a heat sink size of 12 mm $\times$ 12 mm $\times$ 3 mm without constricting flow to much in the cooling channels [30]. Please note that in this case, without any detailed information about size of channel, pressure and airflow velocity inside the cooling channels the thermal resistance of 4°C W^{-1} could be a rough estimation.

2.4 Design

One challenge when building a 12 mm $\times$ 12 mm thermoelectric harvester is the amount of couples that can fit inside. Increasing the number of legs increases the voltage which is important but it also makes the device assembly more complex. And if there is a need of an insulating material or diffusion suppressing material between the legs or electrodes the total volume of thermoelectric material decreases with more couples. In this regard the choice of materials is of big importance as will be explained in the following section.

2.4.1 Materials

To choose the materials in this project the analytical model was used in conjunction with assembly crucial properties like thermal expansion, diffusion- or sublimation suppression. Increasing temperature will affect materials in various ways, like oxidation, sublimation and diffusion. Thermoelectric materials in temperatures as high as 800°C can degrade quickly if not properly cared for. Oxidation can be reduced by proper encapsulation of the device and the individual legs. Finding a suitable encapsulation is however difficult because of the degradation of the encapsulating material itself and that the encapsulating material will have a parasitic effect on the harvester as the material will transfer heat energy through the device.

Sublimation of material means that some or all of the elements in the material leaves the surface. Some materials suffer from rapid sublimation which can degrade the material quickly. The sublimation of a material can in some cases be reduced by encasing the legs in material that acts as a barrier for the sublimating element. This method can reduce the sublimation with a factor of 1000 or more [31].

Diffusion can happen where the thermoelectric material meets the electrode or encapsulating material. Some materials have higher tendency to diffuse than others, so by properly choosing the materials this problem can be reduced. As an example, Sb has a tendency to diffuse into other metals/alloys and form antimonide compounds [32]. In this work Sb is used in the p-type material and the choice of electrode material is therefore crucial. Diffusion can also occur inside the thermoelectric material where single atoms diffuse from their locations. This type of degradation indicates that the temperature is too high for the specific material and a lower temperature or change of material is necessary.

The electrodes can be fitted to the thermoelectric legs in several ways. At low temperature and with insensitive materials it can be soldered or welded. This is not always the best approach, at higher temperatures or with sensitive materials where diffusion bonding can be a better method. Another solution is to not bond the thermoelectric materials with the electrodes and instead press the base plates together to ensure that there is connection. To reduce stress and ensure connection throughout the device the legs should be even and have the same height at operating temperature. One solution is to use springs for every leg to even out the force this way. However, using springs is complicated and can affect the thermal conductance through the device and lower the possible maximum thermal gradient substantially.

The thermoelectric harvester needs two electrically insulating base plates with high thermal

conductivity, see Fig. 2.4. At 800°C the best choice would be SiC with 48 W $m^{-1}K^{-1}$, but with a cost of more than 10 times that of alumina with a thermal conductivity of 7 W $m^{-1}K^{-1}$ calculations were made to see if the higher price would pay off. If using SiGe as thermoelectric material SiC would be a good choice because of the high thermal conductivity of SiGe, see Fig. 2.10. However, with the low thermal conductivity in $Yb_{14}MnSb_{11}$ and $Ba_8Ga_{16}Ge_{30}$ and with alumina sheets as thin as 0.25 mm the difference is only 4 %, see Fig. 2.6. Increasing the thickness to 1 mm would reduce the power output by approximately 17 % using alumina base plates, see Fig. 2.5.

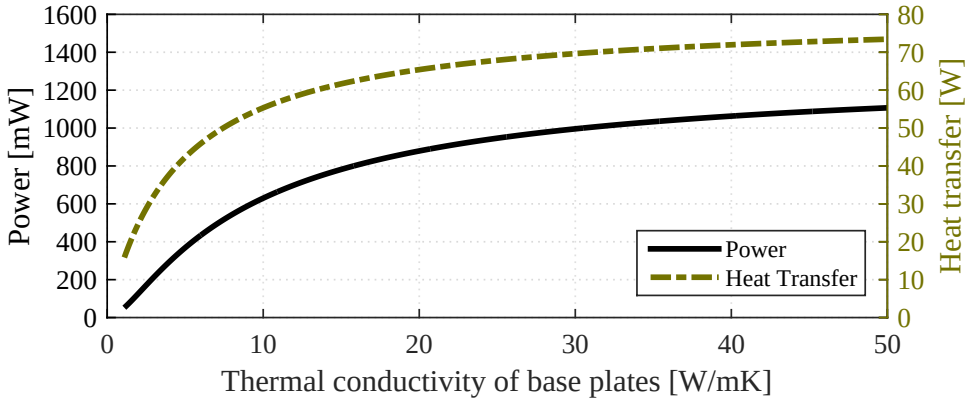

Figure 2.10: Power output and heat transfer through the SiGe generator with increasing thermal conductivity in the base plates. However, because the heat transfer reaches above the maximum 25 W allowed by the heat sink the harvester would not work as intended.

Thermoelectric materials

From calculations the thermoelectric materials $Ba_8Ga_{16}Ge_{30}$ [24, 33] and La-doped $Yb_{14}MnSb_{11}$ [25] gave the best results in the temperature range (600-800°C). The materials figure of merit can be seen in the comparison of different thermoelectric materials, see Fig. 2.1 and 2.2.

Using a synthesis procedure covered in **paper I** the n-type material was synthesized with a highly crystalline material as a result. The melting point of $Ba_8Ga_{16}Ge_{30}$ is approximately 966-974°C and sets the absolute upper temperature limit of the device. However, degradation begins at a lower temperature 725-925°C and depends on the synthesis method [33, 34]. $Ba_8Ga_{16}Ge_{30}$ is sensitive to moisture and oxygen at higher temperatures but is considered to be stable at room temperature. This means that no special measures are needed when cutting or handling the material. The figure of merit for this material is high and at 700°C values above 1.2 has been reported with Seebeck coefficient of -220 μV K^{-1}, electrical resistivity 17 $\mu\Omega$m and thermal conductivity at 1.25 W $m^{-1}K^{-1}$ [24]. The thermal expansion is quite high at 14.2 μm K^{-1} [28].

In **paper I** the synthesis of the p-type material gave less abundant results with some Sn residue left on the crystalline material. La-doped $Yb_{14}MnSb_{11}$ is sensitive to moisture and air and low

levels of oxygen oxidizes the surface. Moreover, the material also reacts with many other materials. Research shows that $Yb_{14}MnSb_{11}$ is stable in contact with alumina, graphite and molybdenum [35, 36, 37]. Using Mo or graphite as an electrode material or as protective layer between the electrode material and $Yb_{14}MnSb_{11}$ is therefore possible. The figure of merit for the La-doped $Yb_{14}MnSb_{11}$ has been reported as high as 1.2 with a Seebeck coefficient of 200 μVK^{-1}, electrical resistivity $7.5{\cdot}10^{-5}$ Ωm and thermal conductivity at 0.6 W $m^{-1}K^{-1}$ [25]. The thermal expansion is higher than $Ba_8Ga_{16}Ge_{30}$ at 16-17.9 μm K^{-1} [38, 39].

2.4.2 Calculations

All calculations include cable losses from the 25 cm long cables discussed in section 2.5.4, with 41.2 mΩ resistance. DC-DC conversion is also included and depends on voltage output with lowest efficiency at 20 mV, giving only 25 % efficiency with Linear Technology LTC3108 [13]. The calculations were done in Matlab.

Leg size

Starting with the size of the thermoelectric legs which is the most important factor when designing a device. Following the equations in **paper II** it is easy to understand that decreasing the leg height will increase heat throughput and power output, see Fig. 2.9. The leg size is therefore pushed to the limit and the area to length ratio 2.6:1 is the size limit for $Ba_8Ga_{16}Ge_{30}$ to handle 200°C without internal stress fracture [28]. Combined with limitation by the maximum heat input of 25 W given by Eq. 2.2 the size of the leg is set to 1.6 mm $\times$ 1.6 mm $\times$ 1 mm.

Electrodes

Because of the p-type material the electrode material is limited to graphite, Mo or Mo-coated material [35]. Graphite electrodes could simplify the fabrication process compared to Molybdenum electrodes with better thermal and electrical contact between the thermoelectric material and the electrode as well as having a less violent reaction to oxygen in high temperatures compared to Molybdenum [40]. However, with a much lower electrical conductivity and the low thermal conductivity in the c-axis the optimum electrode thickness would then be 3.6 mm, see Fig. 2.11[41]. This would make the device thickness 8 mm compared to 1.7 mm for the Mo electrode device and above the weight and size limit decided. Calculations based on molybdenum as electrodes, with resistivity of 220 nΩm at 700°C [42] show that an electrode thickness is in the tens or hundreds of μm for a good weight to power ratio, see Fig. 2.12.

Connecting cables directly to the Mo-electrodes can be done by spot welding but because of the volatile oxidization of Mo this has to be done before closing the device. A more elegant solution that makes it possible to seal the device before attaching cables is to spot weld a less sensitive material (INCO600) to the Mo-electrode, see Fig. 2.13.

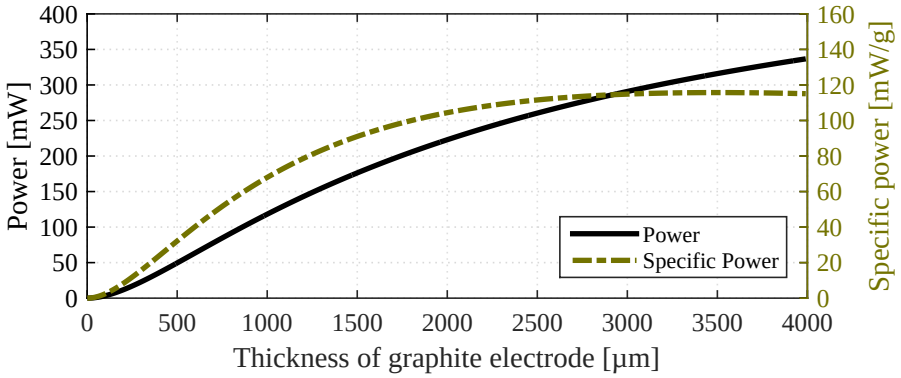

Figure 2.11: The power output and specific power of a 17-couple harvester as a function of the thickness of the graphite electrodes. Maximum specific power is achieved when the electrodes are approximately 3500 μm.

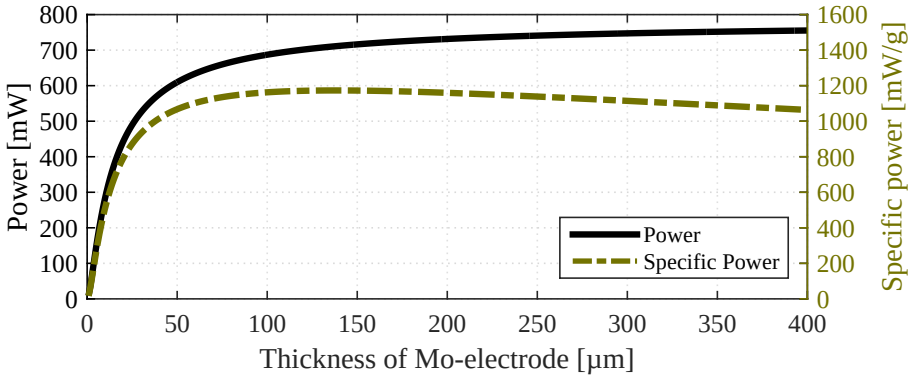

Figure 2.12: The power output and specific power of a 17-couple harvester as a function of the thickness of the Mo-electrodes. For maximum power the electrodes should be as thick as possible, but for maximum power to weight ratio the electrodes should be approximately 50-100 μm.

Sublimation stop

$Yb_{14}MnSb_{11}$ sublimates and Mo-electrodes oxidizes at high temperatures. Therefore, the harvester was fabricated in an oxygen free environment and later also sealed with ceramic glue to not let oxygen or moisture through. The material that surrounds the thermoelectric legs should also keep the sublimation in check. Progress in sublimation repression has been made with alumina paste and is therefore used in this work [43, 35, 31]. When Yb and Sb starts to sublimate, the Sb flows through the alumina and the material starts to degrade, but the Yb is stopped by the alumina and creates a thin layer of Yb that the Sb cannot pass. This method has been showed to reduce the sublimation with a factor of 1000.

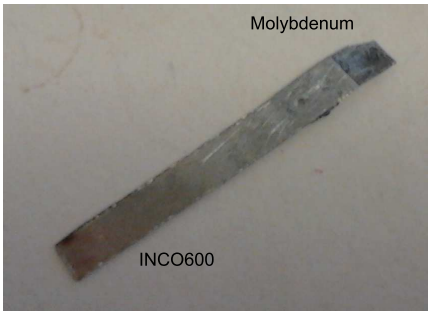

Figure 2.13: Spot welded INCO600 on Mo-electrode. The Mo oxidizes at high temperature, INCO600 does not. This enables two electrodes to be placed outside the harvester and sealing the harvester without attaching cables inside.

2.5 Harvester parts and materials

The materials used in this project were chosen based on both the power output calculations and the material properties, such as physical and chemical durability. A basic device consists of two base plates, electrodes, cables, thermoelectric materials and sealant, see Fig. 2.4.

2.5.1 Alumina substrate

The base plates have the purpose of being a stable build platform and to transfer heat to the thermoelectric material from the surroundings. Alumina is a hard, electrically insulating, inexpensive material with moderate thermal conductivity but can be made very thin. The alumina substrates were delivered in 50 mm x 50 mm plates with a thickness of 0.254 mm.

2.5.2 Thermoelectric legs

When cutting the thermoelectric materials the strategy was to cut pieces small enough that 17 couples would fit in 1.44 mm^2 and still have some room for insulation and sublimation barrier between the legs. Cutting the $Ba_8Ga_{16}Ge_{30}$ to the desired size proved difficult with fragments chipped of the corners, destroying the legs. With limited amount of La-doped $Yb_{14}MnSb_{11}$ and with the risk of exceeding the area-to-height ratio for internal stress the area was not increased beyond 1.6 mm $\times$ 1.6 mm [28]. The decision was to cut both the La-doped $Yb_{14}MnSb_{11}$ and the $Ba_8Ga_{16}Ge_{30}$ to a size of 1.6 mm $\times$ 1.6 mm $\times$ 1 mm, see Fig. 2.14. This gives room for approximately 0.5 mm sublimation barrier between the legs.

To protect the materials from oxygen and moisture during the cutting procedure a coating of wax was applied to the crystals inside the glove box. Also, during the cutting of $Yb_{14}MnSb_{11}$ the cutting fluid was changed from water to hexadecane which produces a protective thin oil coating on the newly cut surfaces of the crystals.

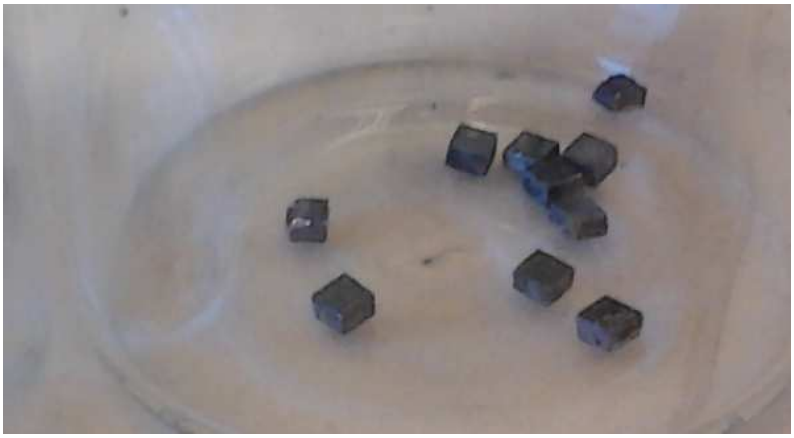

Figure 2.14: The size (1.6 mm $\times$ 1.6 mm $\times$ 1 mm) of the thermoelectric legs in the harvester. The material in this picture is $Ba_8Ga_{16}Ge_{30}$.

2.5.3 Electrodes

Using a pure graphite electrode would make the fabrication process easier with the graphite electrode having the possibility to deform under pressure and keeping the thermoelectric materials intact.

However, the calculations points towards molybdenum being a much better choice. The Mo electrodes was cut from a 80 μm Mo-sheet and glued to the substrate with a very thin layer of high temperature ceramic glue. To improve the connection a 25 μm graphite sheet was placed between the Mo electrode and the thermoelectric material. The outer most electrodes were spot welded to Inco600 alloy, making it possible to seal the device before attaching cables. 2.13.

2.5.4 Cables

The cables were prepared at GKN Aerospace in Trollhättan for this project. One cable contains two thin nickel plated copper wires, these wires are insulated with MgO, has an outer shell of stainless steel and are sealed at the ends with glass. The glass seal is essential to protect the insulation from moisture.

2.5.5 Power management circuit

The desired voltage for the transceiver was 3.3 V. With the relatively low voltage output from the harvester several different types of power management circuits where evaluated and included in the calculations, going as low as 20 mV voltage input and 25 % efficiency with the LTC3108 [13].

2.5.6 Ceramic glue

To seal and protect the materials from oxygen the harvester is encased in two kinds of ceramic glue (Renolit 762 and Thermic 1100) capable of creating a gas impermeable seal up to 800°C respectively 1100°C [44, 45]. The inner glue (Thermic 1100) was applied and cured inside the Argon filled glove box and the Renolit 762 was applied outside the glovebox. Both glues are water soluble, but should maintain the seal under normal conditions given that the Renolit 762 compound is approved and used by both Rolls-Royce PLC® and GKN Aerospace.

2.5.7 Ceramic paste

The thermoelectric legs are separated by a ceramic grid made out of alumina, see Fig. 2.15. The ceramic grid is built from a water based paste (Cotronics Thermeez 7020)which when cured is unsolvable in water [46]. The alumina can operate at up to 1100°C and should act as a sublimation barrier for $Yb_{14}MnSb_{11}$ [35]. The ceramic grid makes it easier to assembly the device and it acts as a glue to keep the harvester intact during assembly. The ceramic grid was made by curing the ceramic paste in a PTFE (Polytetrafluoroethylene) mold pressed against a base plate, see Fig. 2.15.

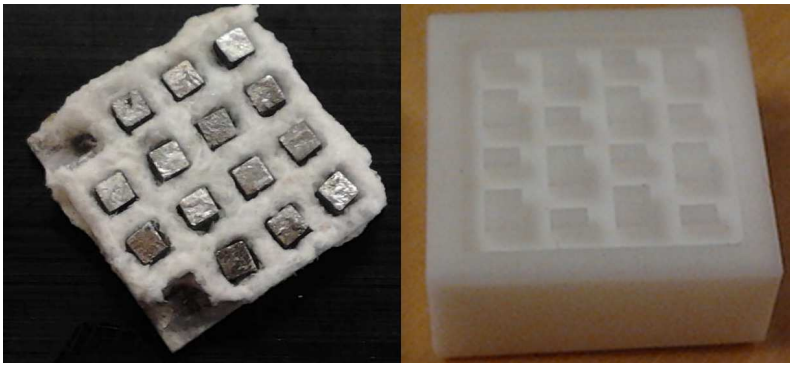

Figure 2.15: The left picture shows a 7-couple ceramic grid made to make assembly easier. The legs in this picture are a bit smaller than the legs used in the actual devices. The picture to the right shows a PTFE mold with an area-ratio of 1:2.6 for $Ba_8Ga_{16}Ge_{30}$:$Yb_{14}MnSb_{11}$.

2.6 Device assembly

A 7-couple device was successfully assembled during the project but this 4-month synthesis and assembly was completely destroyed in an unfortunate accident during the final stage, when sealing with Renolit 762 glue. All voltage measurements on this device were done inside a glovebox without proper temperature measurements. To keep within the project deadlines the decision was to build 1-couple harvesters with the material still available. The assembly of an 1-couple proof-of-concept harvester is explained in **paper I**. The materials used was $Yb_{14}MnSb_{11}$ and

$Ba_8Ga_{16}Ge_{30}$ with 1:1 area-ratio, molybdenum electrodes, alumina base plates, alumina (Thermeez 7020) insulation and INCO600 electrodes spot welded inside the module. The module was sealed with two different ceramic glues.

2.6.1 Electrodes and base plates

The electrodes could not be placed exactly flat and the legs was neither perfectly flat nor of the exact same height. The solution was to make electrodes on one side that could act as compression springs as well, see Fig. 2.16.

Figure 2.16: A schematic figure showing an electrode that has been shaped to act as a spring during first heating. The electrode has some spring force left even when pushed flat.

Most of the compression of the spring electrodes are permanent, when compressing from 0.5 mm thickness to 90 μm it will retract to 190 μm. Measured difference of the height of the legs was below 50 μm. By also including a 25 μm graphite sheet to plastically deform under pressure, the force required for good electrical connection was noticeably reduced.

2.7 Results

Two materials were synthesized, $Ba_8Ga_{16}Ge_{30}$ and La-doped $Yb_{14}MnSb_{11}$. The figure of merit of the materials was estimated using a combination of both measured properties and properties gathered from other work.

The Seebeck coefficient of $Ba_8Ga_{16}Ge_{30}$ reached a top value of 185 μV K^{-1} at 725°C with a resistivity of 3.2 mΩcm. The thermal conductivity was estimated based on previous work using the same method, which has given consistent results on thermal conductivity [24]. Measurements on this batch was not possible due to lack of material.

For the La-doped $Yb_{14}MnSb_{11}$ even less material was available from synthesis and only one measurement was possible on this material, the Seebeck coefficient from room temperature to 207°C. At this temperature the Seebeck coefficient reached 30 μV K^{-1}, one third of previously reported values [47].

Because of the challenges discussed in section 2.5 and 2.6, the assembled thermoelectric energy harvesters had an area ratio of 1:1 and was comprised of one single thermocouple of La-doped $Yb_{14}MnSb_{11}$ and $Ba_8Ga_{16}Ge_{30}$.

2.7.1 Harvester measurements

The measurements were conducted both at Chalmers University and at GKN Aerospace, with higher temperatures and bigger thermal gradients possible at GKN Aerospace.

Low temperature

The low temperature measurement was conducted during the curing of the outermost glue. During the curing procedure the harvester was locked tight between two aluminium blocks, one with active cooling and one acting as heat source. The temperature on the hot side was slowly cooled down from 224°C to 48°C and started with a maximum environmental temperature gradient of 176°C, see Fig. 2.17. The measured voltage from the device reached 18.5 mV, about 70 % of simulated voltage.

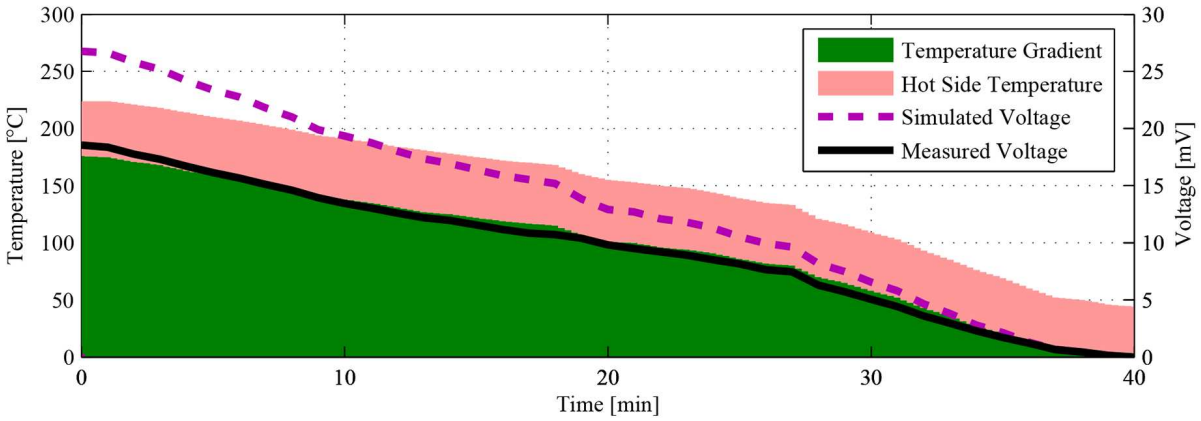

Figure 2.17: Hot side temperature (pink fill) and temperature gradient (green fill) during cool down of the hot side temperature. The measured voltage (black solid line) is compared with the simulated voltage (purple dashed line).

Since the harvester, in one sense, is a thermocouple temperature sensor and the measured Seebeck values was used in the simulations, the actual temperature gradient inside the harvester was about 70% of the environment. Based on the Seebeck values the temperature gradient inside the module reached approximately 123°C.

GKN furnace

At higher temperatures a change of test rig was necessary. The furnace for high temperatures was equipped with an Inco600 rod inserted into the furnace through a hole in the bottom. This rod was used on the cold side of the harvester and the temperature was measured next to the harvester with some thermal isolation on top. A copper heat flange was placed on top of the harvester to absorb and distribute enough heat to the harvester.

The temperature was slowly increased over 180 minutes without active cooling on the inco600 rod, see Fig. 2.18. The thermal gradient was controlled by controlling the temperature increase.

At approximately 280°C and 160°C thermal gradient something happened inside the harvester which reduced the voltage output. The voltage continues to increase as expected after this reduction until 500°C where it suddenly regains the lost efficiency. From 600°C the furnace was

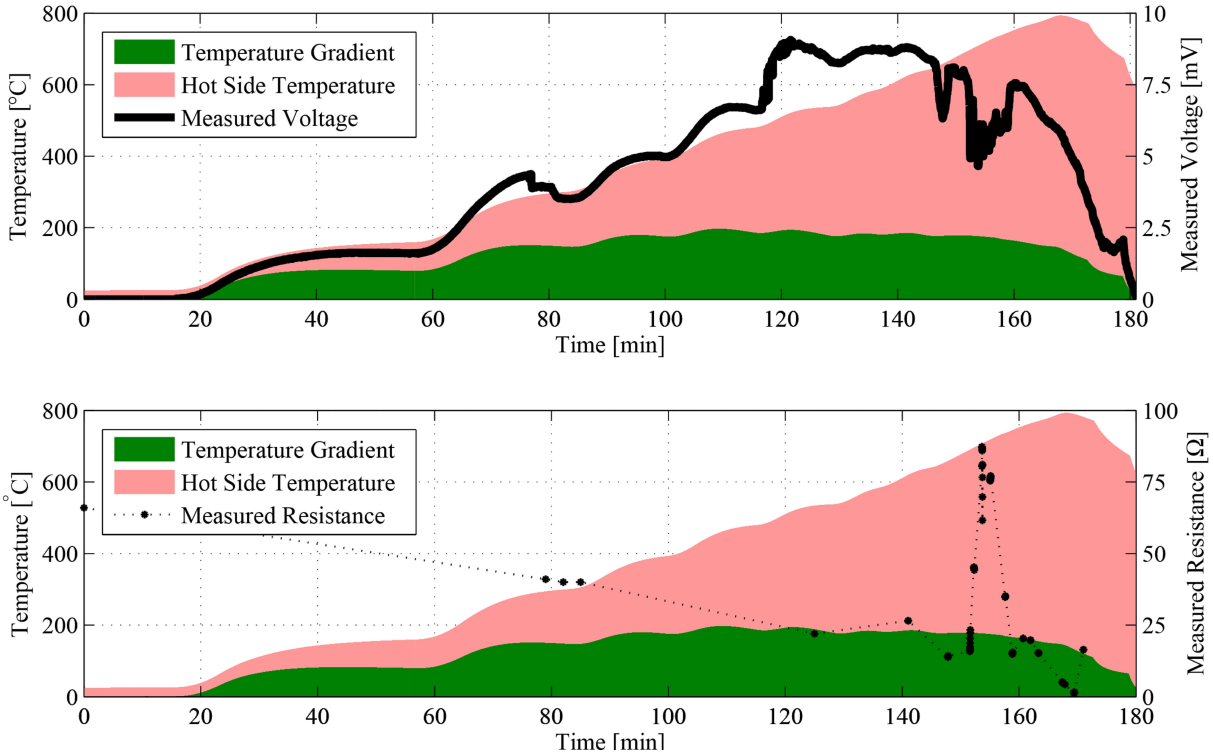

Figure 2.18: Hot side temperature (pink fill) and temperature gradient (green fill) during measurement of harvester voltage and resistance. The measured voltage (black solid line, top figure) show a maximum value of 8.5 mV when the temperature gradient peaks at 200°C. The resistance (points, bottom figure) shows a peak at 750°C during reduced voltage output.

set to full power in an attempt to keep the thermal gradient at 200°C, until 800°C was reached and the furnace was shut down. The voltage dip and increased resistance at 650-750°C indicates that there is insufficient pressure on the harvester legs.

Gas turbine

During the time period when access to the gas turbine was available, no thermoelectric energy harvester was assembled and ready for measurements. A feasibility test was instead done at lower temperatures with a commercial thermoelectric harvester with a size of 40 mm $\times$ 40 mm. The harvester was placed between a copper block and an actively cooled CPU-fan, see Fig. 2.19.

The voltage output from the harvester quickly reached 5 V before melting during the first run. A voltage output over 1.2 V is enough to start the wireless sensor which makes it feasible to power the transceiver without any electronics. During the following tests the harvester was thermally

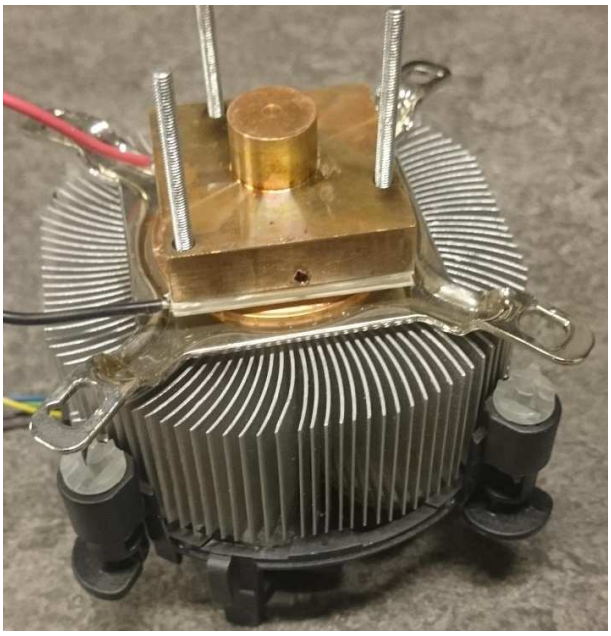

Figure 2.19: A commercial thermoelectric harvester squeezed between a copper block and a CPU block. The copper block was placed on the gas turbine exhaust in an existing mount with the three screws.

insulated to keep the thermoelectric module from melting. When the voltage output reached 1.2 V the wireless sensor started up and sent temperature measurements. Because of the active cooling the harvester could sustain the wireless sensor until turbine shut down.

2.8 Remarks

The Seebeck coefficient measured on the La-doped $Yb_{14}MnSb_{11}$ stopped at 207°C where the thermoelectric rod broke in half. The rod was the only part that was big enough for Seebeck coefficient measurements, but suffered from some visible tin inclusions in the middle of the rod. Although the inclusions looked superficial it is possible that the thermoelectric rod broke because the tin melted and big parts were made of tin, leaving a thin rod of La-doped $Yb_{14}MnSb_{11}$ under pressure. If this is the case then the measured Seebeck coefficient is too low.

All the measurements were performed without thermal paste to improve the thermal conductance to the harvester. For the low temperature measurements thermal paste was possible, but with the harvester so unique and precious it could not be risked to use thermal paste that potentially could damage the harvester before the measurements at GKN Aerospace. The low voltage measured during the high temperature measurement could have the same explanation, with very rough surface on the INCO600 cooling rod. Inspection of the copper heat flange after the measurement also showed a rough and bent surface, distorted by the heat.

To reduce the thermal input during the gas turbine measurement, an insulating block of stainless steel was inserted between the copper block and the exhaust. With this insulation it was possible

to reach above 3 volts and still keep the temperature below the maximum rated 138°C for the harvester. This was however not without problems and if the voltage increase was too slow the transceiver would be locked in start up mode. A system software update should fix this problem. To be certain of success, a switch was included to let the voltage reach 1.2 V, before releasing any power to the transceiver.

CHAPTER 3

Piezoelectric harvester

3.1 Introduction

There are several different types of energy harvester technologies to consider when building a vibrational harvester e.g. electrostatic, electromagnetic, magnetostrictive, triboelectric, piezoelectric and more [48, 49, 50, 51, 49, 52, 53]. In the case of vibrational harvesters, it is not practical to place them in the same location as the thermal harvester in chapter 2, where temperatures reach above 450°C.

Capacitive harvesters does not work well in high temperatures as high temperatures can reduce the electret stability [54]. Magnetostrictive energy harvesters have been shown to work at temperatures of at least 225°C but with some loss in power output at higher temperatures [55]. Work on high temperature piezoelectric energy harvesters have resulted in harvesters capable of 250-300°C, although these harvesters suffers from reduced power output at temperatures above 200°C [56, 57]. Because of this the intended position in the gas turbine was chosen so the vibrational harvester never reaches temperatures above 100°C during a test run.

The gas turbine application calls for a lightweight, broadband energy harvester. With the capability of operation in elevated temperatures, a piezoelectric energy harvester seems like the best choice. Another advantage of building a piezoelectric energy harvester is that most parts needed for the design are available off-the-shelf.

3.2 Piezoelectric materials

The piezoelectric effect arises in some materials when exposed to tension and compression and was first published in 1880 [58]. The source of this piezoelectric effect comes from the crystal structure and how the atoms move under pressure to create a dipole moment. An example of how this dipole moment arises in a quartz crystal can be seen in Fig. 3.1. In rest, each oxygen atom has the same distance to the silicon atoms, but applied stress changes the position and creates a net of dipole moment which causes polarization and an electric field, which is called the piezoelectric effect. There are many different types of crystal structure that give rise to polarization under pressure [59]. One of the most commonly used is the perovskite structure e.g. lead zirconate titanate, $PbZr_{0.5}Ti_{0.5}O_3$ (PZT). PZT are used in the commercial cantilevers used as parts in the harvester designs in **paper III**.

PZT is also ferroelectric which means that below a certain temperature (Curie temperature) the

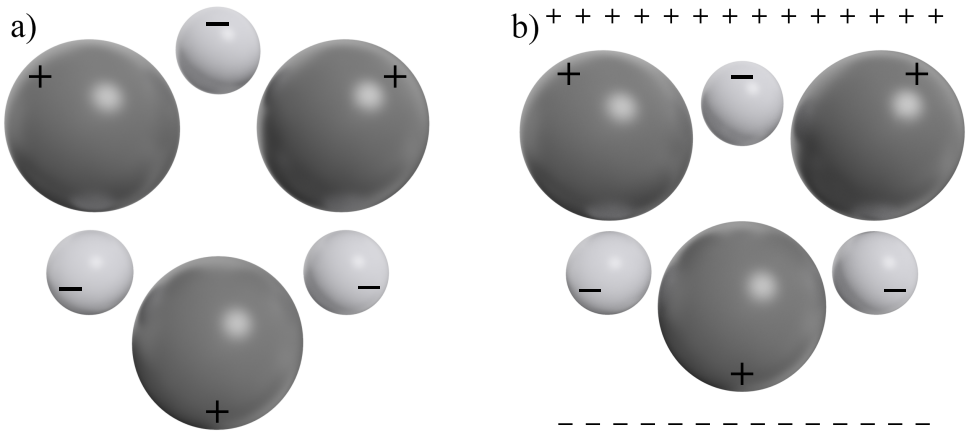

Figure 3.1: Left figure (a): The quartz have no dipole moment when unstressed because of the symmetry. Right figure (b): Piezoelectric effect when quartz is stressed and causes a dipole moment and an electric field.

material have a spontaneous polarization, and that above the Curie temperature the material loses its piezoelectric properties [60]. The spontaneous polarization happens in groups of unit cells and is called Weiss domains [61]. The Weiss domains have random polarization vectors and the average polarization in the material is zero if cooled down without any external electric fields.

When fabricating a piezoelectric material for harvesters the Weiss domains are forced in the same direction by applying an electric field when the temperature is slightly below the Curie temperature. This treatment is called poling and will slightly deform the material to be anisotropic and give it a permanent polarization.

3.3 Harvester design

The basic design of a piezoelectric energy harvester is a cantilever with a thin layer of piezoelectric material on one or both sides of the beam, see Fig. 3.2a. The commercial piezoelectric cantilevers used in **paper III** have a beam of glass fiber reinforced epoxy laminate (FR4) [62], two layers of piezoelectric material and flexible electrodes on each side and one material.

A piezoelectric accelerometer is built to absorb all vibrations equally [63]. This requires that the accelerometer never reaches its resonance frequency because of the amplification created by self-resonance. For a piezoelectric energy harvester the ambition is to have as much amplification as possible. Inspecting the vibration spectrum of the environment gives information on how to design the harvester to have the resonance frequency matched with the most energetic vibrations in the environment.

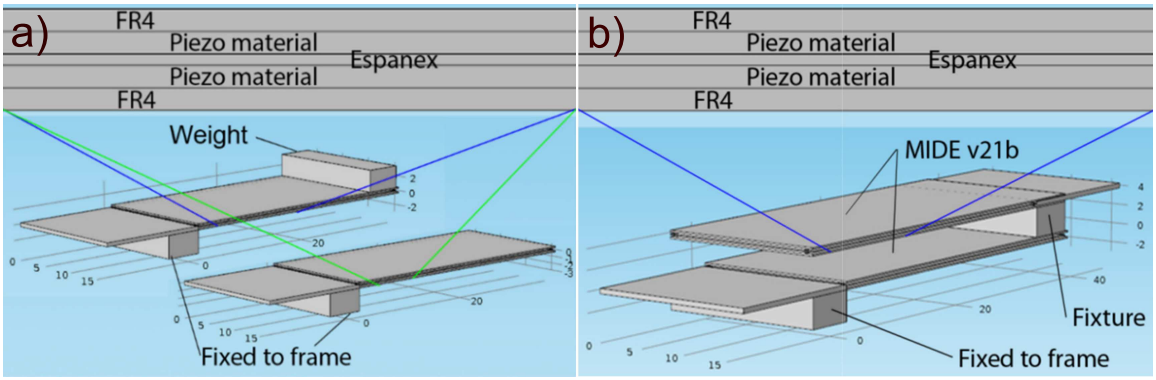

Figure 3.2: Left figure (a): Two single cantilevers, one with tip mass and one without. Both cantilevers are fixed to the frame. Right figure (b): Coupled harvester with the top cantilever fixed to the tip of the bottom cantilever.

For a single degree of freedom (SDOF) system the undamped natural frequency is expressed as follows in Eq. 3.1.

$$\omega_0 = \sqrt{\frac{k}{m}} \tag{3.1}$$

Where ω_0 is the undamped natural frequency, k the effective stiffness of the system and m the effective mass. With the added damping of the system the resonance frequency is expressed as follows in Eq. 3.2.

$$\omega_{res} = \omega_0 \cdot \sqrt{1 - 2\zeta^2} \tag{3.2}$$

3.3.1 Quality factor

If the self-resonance frequency of the harvester matches the vibrations in the environment it is possible to amplify the response in the harvester. This amplification can be made very efficient and reach a factor 200 and more, under the condition that the mass of the environment is far greater than the mass of the harvester [64]. The amplification can be expressed with a quality factor (Q) seen in Eq. 3.3 below.

$$Q = \frac{2\pi E}{\Delta E} \tag{3.3}$$

Where E is the stored energy and ΔE the energy lost each cycle. If the damping is low, the same quality factor can also be expressed as in Eq. 3.4.

$$Q \approx \frac{\omega_{res}}{\Delta\omega} \tag{3.4}$$

where ω_{res} is the resonance frequency (Hz) and $\Delta\omega$ the bandwidth (Hz) [65]. A high quality factor means low losses and high amplification (which of course is a good thing) but it also gives a narrow bandwidth. A narrow bandwidth could be acceptable in some scenarios but in most real world applications this is one of the big challenges with vibrational harvesting.

In our case with the vibrational data available from the gas turbine the frequency at cruise speed varies with several hertz. A broader bandwidth is therefore crucial for this application. Several solutions are available to counter this e.g. to have several cantilevers in an array to cover the entire spectrum, damping or external dampers, moving mass or two-degree-of-freedom coupled harvester [66, 67, 68, 69].

The harvesters presented in this thesis are based on the coupled design to increase the bandwidth, see Fig. 3.2b.

3.3.2 Coupled energy harvester

The energy harvester was assembled with off-the-shelf piezoelectric cantilevers from MIDE. These cantilevers have a fixed resonance frequency that can be tuned by introducing a mass at the tip of the cantilever. The bandwidth is also fixed for the cantilevers but will widen slightly when introducing a tip mass. With two single cantilevers it is possible to cover two different frequencies, either by two different types of cantilevers or by introducing a tip mass, see Fig. 3.2a. Two single cantilevers can therefore give double power output or approximately double the bandwidth depending on the tuning of the cantilevers.

Connecting one cantilever to the end of another cantilever will give a different scenario, see Fig. 3.2b. This design will naturally have two different resonance frequencies for the two cantilevers with a complex relationship between them. The mode forms from this multi-mode harvester design are explained in **paper III**. The folded design with the top cantilever pointing back towards the fixed point, make it possible to have a higher resonance frequency on the bottom cantilever than with a non-folded design. However, it also makes the calibration more difficult and simulations are necessary to calculate the tuning of the harvester.

3.4 Simulations

Attempts were made to find the optimal tuning for the harvester by hand, but the results were less than optimal because of the complexity of the problem. The tuning of the coupled harvester requires specific lengths and tip masses on the cantilevers to give high power output but also specific lengths and tip masses to give correct resonance frequency. These variables do not always match and can give correct resonance frequencies but with low amplification.

To help with the tuning of the harvester, extensive simulations were made with different materials for the couplings and different lengths and tip masses. All simulations are made in COMSOL Multiphysics which is a software for modeling engineering applications [70]. The software uses the finite element method (FEM) to solve the partial differential equations that the specific problem is expressed in.

Simulations show that the coupled harvester in Fig. 3.2b give higher power output than two single cantilevers tuned to the same frequencies, in fact up to 4.7 times higher power output, see Fig. 3.3a. One explanation for this boost in power output is the added mass to the bottom cantilever from the top cantilever. The folded design makes this possible while still maintaining

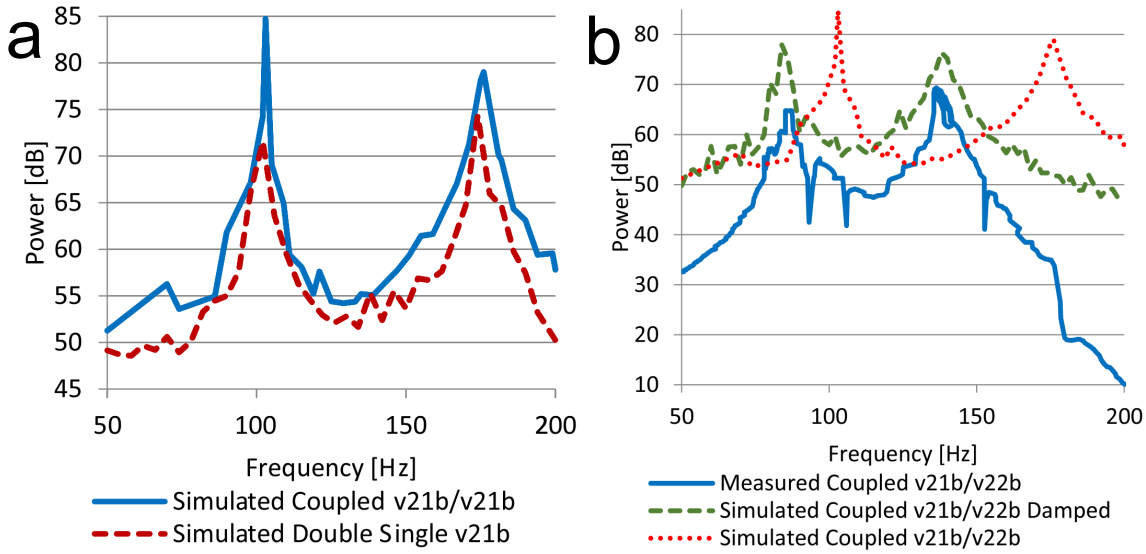

Figure 3.3: Left figure (a): Simulated power output of the coupled harvester (blue solid line) compared with two single cantilevers (red dashed line). Right figure (b): The measured power output (blue solid line) and the simulated power output (red dotted) does not match. Introducing a thin layer (10 μm) of damping material between the couplings and the cantilever gave a more fitting curve (green dashed line).

a relatively high resonance frequency on the bottom cantilever. More insight about the increase in power output comes from inspecting the stress distribution in Fig. 3.4 and the resonance modes in **paper III**.

When inspecting the first resonance mode, when the bottom cantilever in the coupled harvester is in resonance, it can be seen that the coupled design have a more even stress distribution over the piezoelectric material, see Fig 3.4a. In fact, the stress on the bottom cantilever can be made almost perfectly even in simulations. The top cantilever has less stress than the single cantilever but similar shape in the stress distribution with high stress at the fixed point, reduced over the length of the cantilever.

The second resonance mode, when the top cantilever is in resonance, shows an even stress distribution for the bottom cantilever but in this case the bottom cantilever give close to zero power output because of a s-formed shape of the cantilever, see Fig 3.4a and **paper III**. The power output is still higher than from the single cantilevers and with wider bandwidth. This extra amplification comes from the coupling with the bottom cantilever.

3.5 Measurement results

The simulations showed power output up to 4.7 times that of two single cantilevers. To confirm this a piezoelectric energy harvester was assembled and measured upon. The cantilevers in the simulations are based on the off-the-shelf cantilevers from MIDE and the coupling material was tested with both PTFE (Polytetrafluoroethylene) and other aluminium.

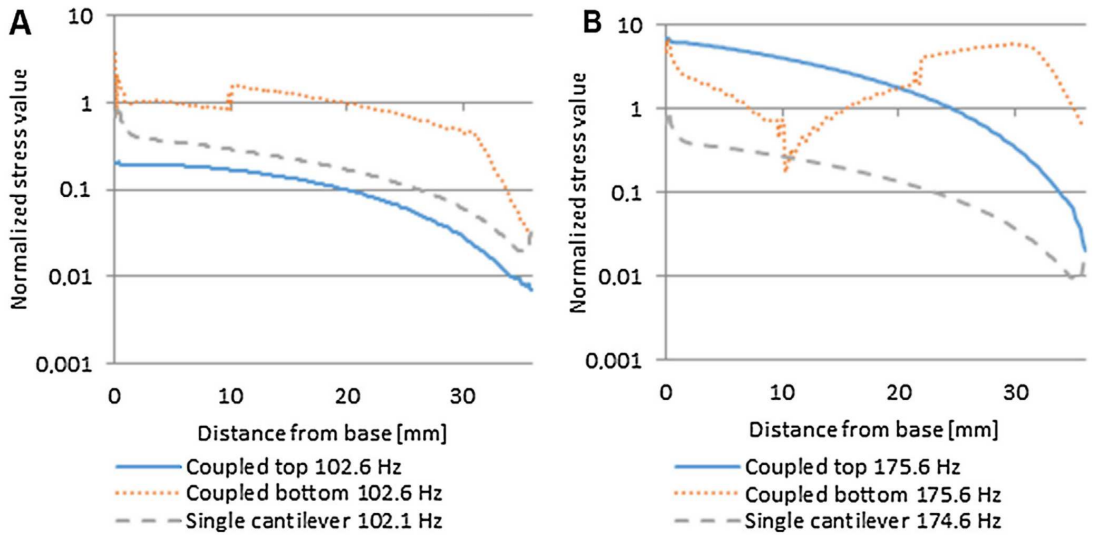

Figure 3.4: Comparison of stress distribution between a single cantilever (grey dashed line), the coupled bottom cantilever (orange dotted line) and the coupled top cantilever (blue solid line). Picture A show the first mode of resonance and B the second mode resonance.

The measurement was done in three different environments. Most of the measurements were undertaken on a shaker table at Chalmers University of Technology. The tuning and the final design corrections were made with the help of this shaker table. Some measurements were made at GKN Aerospace where the shaker rig was equipped with an oven and with the capability of more powerful vibrations. Finally, there were some measurements on an ex-service Rolls-Royce® gas turbine with the harvester connected to a wireless sensor interface.

3.5.1 Shaker table

The measurement setup in the Chalmers lab is a tone generator and a shaker table connected to it. The procedure for the measurements are similar to the simulations, where the harvester is fixed on a shaker table and the frequency is increased in small steps over the frequency span 50-200 Hz.

All the single cantilever and coupled harvester measurements had the same mass on the shaker table to do as little difference in impact on the acceleration profile as possible.

The first obvious difference comparing with the simulations is the lower resonance frequencies in the measurements, see Fig. 3.3b. Based on Eq. 3.1 and 3.2 it can be seen that this behavior points towards lower stiffness and increased damping in the prototype compared to the simulations, with the lower stiffness being the main cause of the lower resonance frequency. This behavior is seen in the simulations despite the use of the same materials in the cantilevers and the same PTFE couplings as the prototype.

By introducing a 10 μm thick layer of soft material between the coupling and the cantilevers in the simulations and thus reducing the stiffness the simulations gave a more fitting result. One

reason why this damping factor can be fitting is that the connection between the cantilever and the coupling is not a perfectly smooth surface and the screws used for clamping is made of PTFE and cannot be too tight, therefore leaving a thin gap of air and rough PTFE islands.

Additional measurements were conducted at GKN Aerospace to inspect two properties of the harvester further, how the harvester will be affected by increased temperature and high acceleration vibrations.

The temperature measurements were conducted under moderate vibrations, giving about 8 V voltage output at room temperature from a single cantilever. With increased temperature the resonance frequency and voltage output dropped slightly, reduced by approximately 2 Hz from 150 Hz and approximately 1-2% voltage output at 100°C. The harvester location in the gas turbine will never reach more than 100°C, far below the rated maximum operating temperature of the cantilevers at 150°C [71].

The harvesters was also subjected to high acceleration vibrations to examine the durability of the harvester design, all under elevated temperatures of approximately 50-70°C. In this violent series of measurements the acceleration was slowly ramped up until something broke. Couplings, solder joints and cables were the first to give up and small redesigns with better fasteners for the couplings and plaited high vibration durable cables were introduced. In the final measurement the harvester reached a maximum possible voltage output of 80 V with approximately 3 g sinusoidal RMS acceleration. With increased acceleration, continuing to 10 g sinusoidal RMS acceleration there were some degradation in the harvester and the voltage output slowly decreased from the initial 80 V to 76 V during a 30 min measurement at 10 g.

3.5.2 Gas turbine

Several trips were made to Rolls-Royce PLC® in Derby, England to measure on an ex-service gas turbine. Even with the data from our previous measurements on the engine as well as the vibrational data from Rolls-Royce® measurements it proved to difficult to prepare the coupled harvesters before arrival, despite having several differently tuned coupled harvesters at our disposal.

None of the coupled harvesters showed the promising power output seen in the simulations and the shaker table experiments. The power output from the harvester was however enough to charge the supercapacitor, start the ZigBee wireless sensor and send the temperature data to the control room for approximately 75 s, see Fig. powerdrain. Attempts to re-tune the harvesters on site was unsuccessful because of the complexity of tuning them by hand. Because of the easy calibration of a single cantilever an attempt to use 10 single cantilevers did reach slightly higher voltage output than the coupled harvesters but still not enough to power the CC2430 ZigBee transceiver [11] for continuous drive. Based on the power requirement of the CC2430 and the power output from the harvesters, showed that the CC2430 can only transmit data once every 2 s.

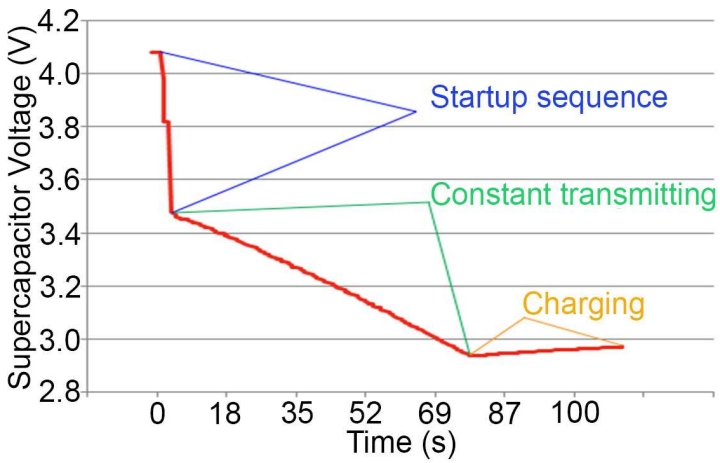

Figure 3.5: The MIDE EHE004 power management releases the power to the CC2430 ZigBee transceiver when the supercapacitor voltage reaches 4.05 V. The start up sequence takes a large part of the available energy in the supercapacitor and is discharged to 2.95 V over the next 75 s with constant transmitting of temperature data. At 2.95 V the power management cuts power and the supercapacitor starts to charge again.

3.6 Remarks

The difference between the measurements and the simulations was substantial without the soft layer in the simulations. Adding a soft layer reduced the stiffness and the difference in resonance between the simulation and the measurement but it is not an elegant solution. After publishing **paper III** the couplings was improved significantly by replacing the PTFE with small electrically isolated metal screws and aluminium blocks. This moved the measured resonance frequencies closer towards the simulated values, making it easier to tune, but the added mass reduced the available frequency span.

CHAPTER 4

Supercapacitor

4.1 Introduction

A conventional capacitor consists of two conductive plates separated by an insulator (dielectric). Increasing the area of the plates, reducing the distance between the plates or increasing the dielectric strength of the insulator will increase the capacitance of the capacitor. The energy density (E) of a capacitor can be expressed by the capacitance (C) and the voltage (V) as follows from eq. 4.1.

$$E = \frac{CV^2}{2} \tag{4.1}$$

Supercapacitors also have two electrodes, but instead of a solid dielectric medium between the electrodes the supercapacitor has an electrolyte. To protect the electrodes from short circuit and still keep the electrolyte capable of reaching both electrodes, an ion permeable electrically insulating separator is placed between the electrodes, see Fig. 4.1. The electrodes also differ from those in a conventional capacitor, having a porous high surface area (usually more than 1000 m^2/g) [72].

The high surface area in the electrodes gives a high capacitance if utilized. The pore size of the electrode material and the ions in the electrolyte determines how much of the material that can be utilized. Electrolytes can be aqueous, organic or ionic liquids. Ionic liquids are molten salts that are in liquid form in room temperature. The electrolyte also determines the voltage of a supercapacitor and range from 1.23 V for aqueous electrolytes to 4 V for ionic liquids [73, 74].

With applied voltage on the supercapacitor ions will diffuse into the electrode pores and accumulate on the electrode surface of opposite charge. These layers (double layer) of charge have a very small distance between them and in combination with the high surface area this gives supercapacitors approximately 10-100 times higher energy density [75, 76].

Even with this substantial increase in energy density, it is not enough to challenge the energy density of batteries. However, with no chemical reaction in a supercapacitor the power density is higher and the cycle life is much higher than batteries and can reach more than 10 million cycles compared to approximately 1000 for batteries [77].

With the increased power density and increased cycle life it can (in some scenarios) be beneficial to combine a high power density supercapacitor with a high energy density battery to charge the supercapacitor from the battery and handle high power fluctuations with the supercapacitor.

A more powerful combination is to combine a supercapacitor with an energy harvester as power source. In **paper IV** a supercapacitor is assembled with the aim for high temperature application

in combination with the energy harvester solutions discussed in **paper I** and **paper III**.

A supercapacitor capable of operation in 800°C would be optimal for the thermoelectric harvester but is difficult to achieve. Because of the need of electronics the primary goal is to reach a temperature higher than the electronics can handle.

Military (and aerospace) standard for electronics is 125°C, but of course this is the minimum requirement and higher temperatures are always welcome [78]. The demand for high temperature electronics goes even higher in the oil drilling industry where the electronics need to handle 200°C [79]. At this temperature there are very few solutions available and going beyond 200°C leaves only silicon carbide electronics, capable of up to 600°C.

Organic and aqueous electrolytes are excluded at temperatures above 125°C because of their low boiling points. Ionic liquids can handle temperatures far beyond 125°C [80] but with the drawback of higher viscosity which leads to reduced capacitance and lower power density [81]. Increasing the temperature to 120°C from room temperature will decrease the viscosity by a factor of 32 [82].

For long term use it is important that the electrolyte have low corrosive effect on the other materials in the supercapacitor. The corrosive effect will increase with increased temperature.

4.2 Assembly

The objective was to build a functional proof-of-concept supercapacitor that could be combined with an energy harvester. Temperature stability was one of the main points when choosing materials.

The electrolyte is the most difficult part, especially for a 800°C supercapacitor. The choice of electrolyte is 1-Ethyl-3-methylimidazolium acetate (EMIM Ac), an ionic liquid capable of temperature well above 125°C. The maximum operating temperature of pure EMIM Ac is 181°C, but depending on the materials it interacts with this temperature can be lower [83].

The electrodes are made of activated carbon (Kuraray® , YP-80F), carbon black and PTFE binder with the weight ratio 80:10:10. The PTFE binder reduces the maximum operating temperature of the electrode to approximately 300°C, a non existing problem as long as the electrolyte sets the upper limit.

The collectors are made of stainless steel foil and the separator is a glass microfiber filter (Whatman ®). Tests show that the separator can handle more than 300°C [84].

The parts are assembled with two carbon electrodes on each side of a glass fiber separator, with the collectors connected to the electrodes, see Fig. 4.1.

Of course, a functional supercapacitor needs to be hermetically sealed to keep the electrolyte. The assembly was first done with ceramic encasement with successful result but unnecessary expensive and tedious for temperatures below 260°C. A cheaper and simpler polyimide film (Kapton ® [85]) with silicone adhesive capable of up to 260°C was used during the measurements with the added benefit of flexibility, see Fig. 4.1 and 4.2.

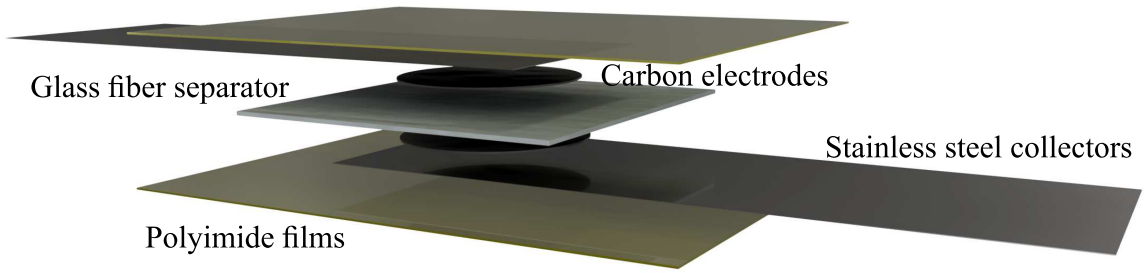

Figure 4.1: Schematic of a supercapacitor with a glass fiber separator in the middle, separating the two carbon electrodes. The collectors are attached to the carbon electrodes and finally everything is sealed between the two sheets of polyimide film with silicone adhesive.

4.3 Measurements

A small oven, capable of 300°C and *in situ* measurements, was built and placed close to the measurement equipment (Gamry Reference 3000AE) with the supercapacitor placed inside, see Fig. 4.2. Two measurements were conducted on two separate supercapacitors. The first

Figure 4.2: The supercapacitor inside a small oven capable of 300°C. The supercapacitor is placed inside a small vise to keep pressure on the electrodes during the measurement.

measurement examines the component degradation from a temporary high temperature heat treatment. The supercapacitor was subjected to 190°C for 2 h with capacitance measurements before and after. The heat treatment showed no degradation of the components, instead a slightly increased capacitance after cool down that could be a result from increased wetting.

The second measurement was made *in situ* to examine temporary loss or increase of capacitance during exposure at elevated temperatures, see Fig. 4.3. Also, an excessive heat treatment at 250°C was conducted to see the effect of decomposition.

The supercapacitor for the second measurement was heat treated at 150°C for more than 2 h before the measurement to reduce the effect of increased capacitance seen in the first measurement. The temperature was then lowered and held at 37°C until the cyclic voltammetry measurement reached steady state with 57 mF capacitance measured. During the following temperature increase to 178°C, the capacitance increased and the maximum voltage slowly decreased. It has later been shown that the voltage limit is reduced from 1.5 V at room temperature to 1.3 V at 150°C [86].

When the temperature reached 178°C it was held for 2 h and reached a steady state capacitance of 92 mF, an increase of 61% compared to 37°C. The temperature was now further increased to 250°C where it is certain that decomposition takes place. Inspection of the cyclic voltammogram show some non-electrostatic reactions (a hump at 0.4 V) that indicates degradation, Fig. 4.3. The degradation could also be seen visually with a color change of the capacitor.

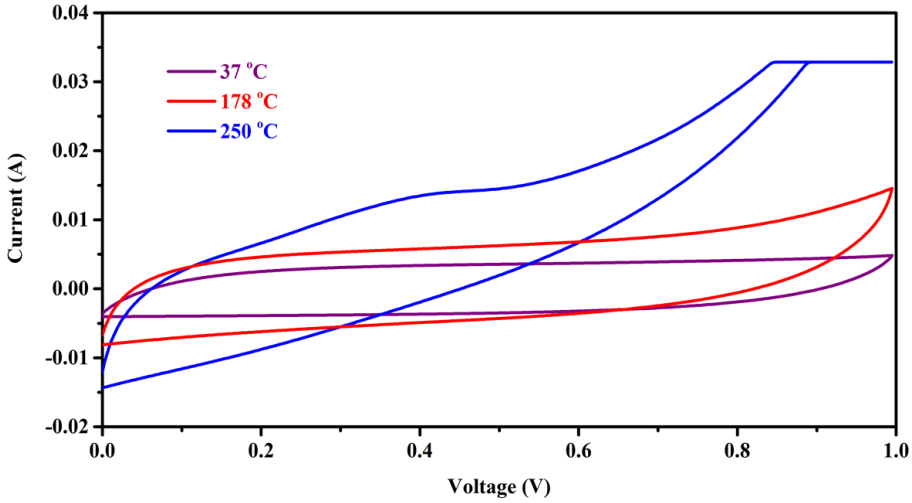

Figure 4.3: Cyclic voltammogram from three different temperatures, 37°C, 178°C during 2 h and 250°C during 10 min. The measurement at 37°C showed a capacitance of 57 mF, when increased to 178°C the capacitance increased by 61% to 92 mF. The final 250°C heat treatment showed signs of degradation of the supercapacitor, but still no capacitive loss after cooling down.

The first measurement shows that the supercapacitor gains permanently increased capacitance from the heat treatment, possibly because of the reduced viscosity, resulting in better wetting. The second measurement shows increased capacitance during exposure to elevated temperatures. The increase is substantial, but the increase in energy density is not equally big because of the lower voltage limit.

4.4 Remarks

The cycle life at 178°C is not investigated in **paper IV** but further investigation show that EMIM Ac have 85% retention at 1000 cycles when kept at 150°C [86].

The excessive heat treatment resulted in greatly increased capacitance, but also visible degradation. Despite the degradation the capacitance was increased and after 10 minutes of excessive heat the supercapacitor was cooled down to 178°C again with slightly increased capacitance than before. The amount of degradation and the effect of the degradation on the supercapacitor was not investigated.

CHAPTER 5

Discussion, conclusion and outlook

5.1 Discussion

The low temperature measurement on the thermoelectric harvester reached only about 70% of the simulated value. With the thermoelectric harvester containing one thermocouple with measured Seebeck coefficients it also acts as a thermoelectric temperature sensor. The sensor does not measure the temperature of the environment or even the temperature gradient of the environment, it measure the temperature gradient of the thermoelectric legs inside the energy harvester. The temperature gradient reached approximately 123°C based on the measured Seebeck coefficients. The rest of the temperature gradient is lost in the base plates, the electrodes and all the contact interfaces between the environment and the thermoelectric legs.

The reduced voltage output (8.5 mV versus 75 mV in simulations) during the high temperature measurement indicates a bad contact inside the harvester. Unfortunately no resistance measurement was done close to the first voltage drop at 280°C, see fig 2.18. During the second voltage drop measurements on the resistance show a correlation between the resistance and the reduced voltage. A probable explanation to the bad contact comes from the copper heat flange, acting as both a thermal transfer unit and a mass to maintain pressure on the thermoelectric legs. With the apparent distortion at higher temperatures the pressure on the legs could be uneven and give bad contact.

The piezoelectric harvester results on the gas turbine did not give the power output predicted by the shaker table or the simulations. There are a few possible explanations for this behavior. One of the more likely reasons why it performed poorly is the encapsulation box and the mounting of the box to the gas turbine. The mounting was far from optimal and could possibly be a big damping factor of the entire system. The box itself also made an impact on the resonance frequency and depending on how the box was oriented it gave different results despite the use of a similar mounting method. Tuning the harvesters at site proved to be too difficult even with the pre-tuned markers and different settings prepared with simulations.

The cycle life of the supercapacitor at 178°C is not investigated in **paper IV** but further investigation show that EMIM Ac have 85% retention at 1000 cycles when kept at 150°C [86]. The excessive heat treatment resulted in greatly increased capacitance, but also visible degradation. Despite the degradation the capacitance was increased and after 10 minutes of excessive heat the supercapacitor was cooled down to 178°C again with slightly increased capacitance than before. The amount of degradation and the effect of the degradation on the supercapacitor is not investigated.

5.2 Conclusion

The goal in this thesis was to power a wireless sensor node on a gas turbine with energy harvesting, and transmitting temperature data to a computer in a control room nearby. Two different energy harvester concepts were undertaken, a coupled vibrational energy harvester with increased bandwidth and a thermoelectric energy harvester for the temperature span 600-800°C. For energy storage a supercapacitor capable of temperatures up to 178° was investigated. The power management circuit and the transceiver was bought off-the-shelf.

A thermoelectric energy harvester was designed and built using in-house synthesized n-type and p-type materials. The intended design with 1:3.7 area ratio was abandoned due to lack of material and replaced with 1:1 area ratio, giving the design 84% of the planned power output. The measurements in low temperature and high temperature gave results below simulated values and no power measurements or gas turbine measurements were conducted with the thermoelectric harvester.

The second harvester type was the coupled piezoelectric energy harvester, designed to have increased bandwidth without losing power output. The design is quite durable in the current form, capable of withstanding powerful vibrations. When subjected to vibrations with 10 g RMS, the harvester showed 5% degradation over 30 min, but did not break. These kind of vibrations will never occur in any engine unless it is catastrophically unbalanced.

For the coupled piezoelectric energy harvester it is crucial to store the energy to be able to power up the transceiver. The goal for the supercapacitor is to operate in temperatures beyond what batteries can handle (125-150°C). The maximum temperature of 181°C that the electrolyte (EMIM Ac) can handle, was the minimum temperature of which the other materials were based. The measurements show that the supercapacitor can operate in elevated temperatures and actually gain 61% capacitance when the temperature is increased from 37°C to 178°C.

The gas turbine measurements were made with the coupled piezoelectric harvester and a commercial thermoelectric harvester. The piezoelectric harvester was connected to a power management circuit and managed to power the transceiver for 75 s before the commercial supercapacitor was empty. The continuous sending could not be sustained with the piezoelectric harvester. The power output from the harvester could only power the transceiver with 2 s delay between transmission, which is still enough for the application.

The commercial thermoelectric energy harvester was more powerful than the piezoelectric harvester and it was possible to start up and send temperature data with the transceiver, even without any power management or energy storage. The commercial harvester could easily power the transceiver, and if combined with an intelligent system for power distribution a single thermoelectric harvester could power tens of wireless sensors nodes.

5.3 Outlook

No power measurements were conducted on the thermoelectric energy harvester. Before conducting any power output measurements it is important to solve the contact issue. The connection of the electrodes to the $Yb_{14}MnSb_{11}$ material can be done by diffusion bonding [87], i.e. heating the materials to 1000°C under high pressure during 12 hours. This is a temperature higher than $Ba_8Ga_{16}Ge_{30}$ can handle so the diffusion bonding needs to be done on $Yb_{14}MnSb_{11}$ separately, before assembly of the device. Diffusion bonding between titanium and other metals can be made at much lower temperatures than 1000°C and bonding a thin layer of Ti with the Mo-electrode can be done at low pressures and 700°C [88]. It is however not known if $Ba_8Ga_{16}Ge_{30}$ can be bonded with Ti without problems.

For the vibrational energy harvester it could be beneficial to design it for 200°C and above to increase the possible locations for harvesting in a gas turbine. When combining it with a supercapacitor it is feasible as a power source as long as the supercapacitor can handle the temperature. With a 61% capacitance increase when increasing the temperature from 37°C to 178°C an electrolyte with even higher temperature stability is interesting.

References

[1] CORDIS, "Sensors Towards Advanced Monitoring and Control of Gas Turbine Engines," *CORDIS*, vol. 314061, 2012-2016.

[2] X. Luo, J. Wang, M. Dooner, and J. Clarke, "Overview of current development in electrical energy storage technologies and the application potential in power system operation," *Applied Energy*, vol. 137, pp. 511–536, 2015.

[3] S. Pay and Y. Baghzouz, "Effectiveness of Battery-Supercapacitor Combination in Electric Vehicles," *IEEE Bologna Power Tech Converence*, vol. 23-26 July, 2003.

[4] J.-P. Im, S.-W. Wang, S.-T. Ryu, and G.-H. Cho, "A 40 mV Transformer-Reuse Self-Startup Boost Converter With MPPT Control for Thermoelectric Energy Harvesting," *IEEE Journal of Solid-State Circuits*, vol. 47, 12, pp. 3055–3067, 2012.

[5] J. Roberts, "Discussions," *Rolls-Royce PLC*, vol. May 22-23, 2013.

[6] M. Yuri, J. Masada, K. Tsukagoshi, E. Ito, and S. Hada, "Development of 1600°C-Class High-efficiency Gas Turbine for Power Generation Applying J-Type Technology," *Mitsubishi Heavy Industries Technical Review*, vol. 50, 2013.

[7] L. Bodenes, R. Naturel, H. Martinez, R. Dedryvère, M. Menetrier, L. Croguennec, J.-P. Pérès, C. Tessier, and F. Fischer, "Lithium secondary batteries working at very high temperature: Capacity fade and understanding of aging mechanisms," *Journal of Power Sources*, vol. 236, p. 265275, 08 2013.

[8] J. Eriksson and S. Fagerholm, "Exhaust Analyser for Simplified Emissions Testing on Heavy Duty Vehicles," *Master of Science Thesis*, 2014.

[9] M. Duff and J. Towey, "Two Ways to Measure Temperature Using Thermocouples Feature Simplicity, Accuracy, and Flexibility," *Analog Dialogue*, vol. 44-10, 2010.

[10] J. Kemp, E. Gaura, M. Allen, and J. Brusey, "Optimising low power dual prediction systems," *Conference: the 6th ACM workshop*, pp. 7–10, 11 2015.

[11] CC2430, "A True System-on-Chip solution for 2.4 GHz IEEE 802.15.4 / ZigBee," *Texas Instruments: Data sheet*, 2014.

[12] MIDE, "EHE004: Energy harvesting electronics," *Data Sheet, rev 2*, 2013.

[13] Datasheet, "LTC3108, Ultralow Voltage Step-Up Converter and Power Manager," *Linear Technology Corporation*, 2010.

[14] T. J. Seebeck, "Magnetische Polarisation der Metalle und Erze durch Temperatur-Differenz," *Abhandlungen der Königlichen Akademie der Wissenschaften zu Berlin*, vol. 265, 1822-1823.

[15] L. Baranowski, J. Snyder, and E. Toberer, "Concentrated solar thermoelectric generators," *Energy Environ. Sci.*, vol. 5, 9055, 2012.

[16] CAP-xx, "Energy Storage Technologies," *cap-xx*, 2018. [Online]. Available: https://www.cap-xx.com/resource/energy-storage-technologies/

[17] R. Vullers, R. Von Schaijk, C. Van Doms, and R. Mertens, "Micropower Energy Harvesting," *Solid-State Electronics*, vol. 53, pp. 684–693, 2009.

[18] TECTEG, "MFR," *TECTEG*, 2013. [Online]. Available: http://thermoelectric-generator.com/teg-cascade-800c-hot-side-thermoelectric-power-modules/

[19] G. L. Bennett, "Space Nuclear Power: Opening the Final Frontier," *4th IECEC*, vol. 26-29 June 2006, pp. AIAA 2006–4191, 2006.

[20] N. S. Hudak and G. G. Amatucci, "Small-scale energy harvesting through thermoelectric, vibration, and radiofrequency power conversion," *J. Appl. Phys*, vol. 103, pp. 101 301–1–24, 2008.

[21] TEGpower, "http://www.tegpower.com/index.html," -, vol. -, p. 4 july 2013, 2013.

[22] T. M. Tritt, "Thermoelectric Materials: Principles, Structure, Properties, and Applications," *Encyclopedia of Materials: Science and Technology*, vol. 2, pp. 1–11, 2002.

[23] J. Snyder and E. Toberer, "Complex thermoelectric materials," *Nature Materials*, vol. 7, pp. 105–114, 2008.

[24] A. Palmqvist and et al., "Large thermoelectric figure of merit at high temperature in Czochralski-grown clathrate $Ba_8Ga_{16}Ge_{30}$," *Journal of Applied Physics*, vol. 99, 023708, 2006.

[25] E. Toberer, S. Brown, S. Kauzlarich, and J. Snyder, "High thermoelectric efficiency in lanthanum doped $Yb_{14}MnSb_{11}$," *Applied Physics Letter*, vol. 93, 062110, 2008.

[26] B. Sherman, R. R. Heikes, and R. W. Ure, "Calculation of Efficiency of Thermoelectric Devices," *American Institute of Physics*, vol. 31, no. 1, 1960.

[27] H. Zhu, "Aluminathermal," *INSA de lyon*, 2011.

[28] N. L. Okamoto, T. Nakano, K. Tanaka, and H. Inui, "Mechanical and thermal properties of single crystals of the type-I clathrate compounds Ba8Ga16Ge30 and Sr8Ga16Ge30," *Journal of Applied Physics*, vol. 104, pp. 013 529–1–7, 2008.

[29] S. Song, S. Lee, and V. Au, "Closed-Form Equation for with Variable Thermal Constriction/Spreading Resistance Boundary Condition," *1994 IEPS CONFERENCE*, pp. 111–121, 1994.

[30] S. Lee, "Optimum Design and Selection of Heat Sinks," *Eleventh IEEE SEMI-THERMN Symposium*, 1995.

[31] J. Paik and T. Caillat, "Alumina paste sublimation suppression barrier for thermoelectric device," *United states patent application publication*, vol. US 2010/0229910 A1, p. Sep. 16 2010, 2010.

[32] E. Wiberg, N. Wiberg, and A. Holleman, "Inorganic Chemistry," *Academic Press*, 2001.

[33] A. Saramat, E. Toberer, A. May, and J. Snyder, "Thermal stability and phase purity in polycrystalline $Ba_8Ga_xGe_{46-x}$," *Journal of Electronic Materials*, vol. vol 38, No. 7, pp. 1423–1426, 2009.

[34] M. Christensen, J. Snyder, and B. B. Iversen, "Degradation of BaGaGe," *International Conference on Thermoelectrics*, pp. 40–44, 2006.

[35] J. Paik, E. Brandon, T. Caillat, P. Ewell, and J. Fleurial, "Life testing of $Yb_{14}MnSb_{11}$ for high performance thermoelectric couples," *Proceedings of Nuclear and Emerging Technologies for Space*, vol. (2011), 2011.

[36] S. Firdosy, B. Li, V. Ravi, J. Sakamoto, T. Caillat, R. Ewell, and E. Brandon, "Metallization for $Yb_{14}MnSb_{11}$-Based Thermoelectric Materials," *Tech Briefs*, vol. Aug 1, 2011.

[37] J. Paik, E. Brandon, T. Caillat, R. Ewell, and J. Fleurial, "Life Testing of $Yb_{14}MnSb_{11}$ for High Performance Thermoelectric Couples," *Proceedings of Nuclear and Emerging Technologies for Space*, 2011.

[38] V. Ravi, S. Firdosy, T. Caillat, E. Brandon, K. Van Der Walde, L. Maricic, and A. Sayir, "Thermal expansion studies of selected high-temperature thermoelectric materials," *Journal of Electronic Materials*, vol. 38, no 7, pp. 1433–1442, 2009.

[39] V. Ravi, S. Firdosy, T. Caillat, E. Brandon, K. V. D. Walde, L. Maricic, and A. Sayir, "Thermal Expansion Studies of Selected High Temperature Thermoelectric Materials," *JPL Technical Report Server*, vol. 45331, 2014.

[40] E. S. Jones, J. F. Mosher, R. Speiser, and J. W. Spretnak, "The Oxidation of Molybdenum," *Corrosion*, vol. 14, pp. 20–26, 1957.

[41] K. Sun, M. A. Stroscio, and M. Dutta, "Graphite c-axis thermal conductivity," *Superlattices and Microstructures*, vol. 45, no. 2, pp. 60 – 64, 2009. [Online]. Available: http://www.sciencedirect.com/science/article/pii/S0749603608002644

[42] C. K. Gupta, "Extractive Metallurgy of Molybdenum," *CRC Press*, pp. 6–8, 1992.

[43] J. Paik and T. Caillat, "Alumina paste layer as a sublimation suppression barrier for $Yb_{14}MnSb_{11}$," *NASA Tech Briefs*, vol. aug, pp. 22–23, 2010.

[44] Fuchs, "Renolit 762 High Temperature Jointing Compound," *Fuchs*, vol. November, 2008.

[45] Steffca, "Thermic 1100," *Steffca*, 2010.

[46] Datasheet, "Thermeez 7020 Ceramic Putty," *Cotronics Corporation*, 2001.

[47] E. S. Toberer, S. R. Brown, T. Ikeda, S. M. Kauzlarich, and G. J. Snyder, "High thermoelectric efficiency in lanthanum doped $Yb_{14}MnSb_{11}$," *Applied Physics Letters*, vol. 93, no. 6, p. 062110, 2008. [Online]. Available: https://doi.org/10.1063/1.2970089

[48] L. Dhakar, "Triboelectric Devices for Power Generation and Self-Powered Sensing Applications," *Springer; 1st ed. 2017 edition*, 2017.

[49] S. P. Beeby, M. J. Tudor, and N. M. White, "Energy harvesting vibration sources for microsystems applications," *Meas. Sci. Technol.*, vol. 17, pp. R175–R195, 2006.

[50] Y. Chiu and V. F. G. Tseng, "A capacitive vibration-to-electricity energy converter with integrated mechanical switches," *J. Micromech. Microeng.*, vol. 18, pp. 104 004, 1–8, 2008.

[51] J. Huang, R. O'Handley, and D. Bono, "High efficiency vibration energy harvester," Jan. 10 2006, uS Patent 6,984,902. [Online]. Available: https://www.google.com/patents/US6984902

[52] T. Krupenkin and J. A. Taylor, "Reverse electrowetting as a new approach to high-power energy harvesting," *Nature Communications*, vol. 2, p. 448, 2011.

[53] S. Roundy and P. K. Wright, "A piezoelectric vibration based generator for wireless electronics," *Smart Mater. Struct.*, vol. 13, p. 11311142, 2004.

[54] S. Boisseau, G. Despesse, and B. A. Seddik, "Electrostatic Conversion for Vibration Energy Harvesting, Small-Scale Energy Harvesting," *InTech*, 2012. [Online]. Available: https://www.intechopen.com/books/small-scale-energy-harvesting/electrostatic-conversion-for-vibration-energy-harvesting

[55] J.-H. Yoo, A. Flatau, and A. Purekar, "Performance of galfenol energy harvester at high temperature," *ASME 2011 Conference on Smart Materials, Adaptive Structures and Intelligent Systems, SMASIS 2011*, vol. 1, 01 2011.

[56] J. Wu, H. Shi, T. Zhao, Y. Yu, and S. Dong, "High-temperature $BiScO_3$-$PbTiO_3$ piezoelectric vibration energy harvester," *Advanced Functional Materials*, vol. 26, no. 39, pp. 7186–7194, 2016. [Online]. Available: http://dx.doi.org/10.1002/adfm.201602645

[57] S. Barker, K. V. Vassilevski, N. G. Wright, and A. B. Horsfall, "High temperature vibration energy harvester system," in *2010 IEEE Sensors*, Nov 2010, pp. 300–303.

[58] J. Curie and P. Curie, "Phénomènes électriques des cristaux hémièdres à faces inclinées," *J. Phys. Theor. Appl.*, vol. 1, pp. 245–251, 1882.

[59] P. Dineva, D. Gross, R. Mller, and T. Rangelov, "Dynamic Fracture of Piezoelectric Materials: Solution of Time-Harmonic Problems via BIEM," *Springer Science & Business Media*, 2014.

[60] J. Valasek, "Piezoelectric and allied phenomena in Rochelle salt," *Phys Rev*, vol. 15, p. 537, 1920.

[61] J. W. Waanders, "Piezoelectric Ceramics: Properties & Applications Chapter 2: Physical Basis," *Chapter 2*, 1991.

[62] Datasheet, "Volture products - Material Properties," *Volture*, p. 2, 2010. [Online]. Available: http://shared.damianomilani.com/tesi/mide/volture_material_properties_2010.pdf

[63] Gracey, "Piezoelectric Accelerometers Theory and Application," *Metra Mess- und Frequenztechnik*, 2001.

[64] T. Manzaneque, J. Hernando-Garca, A. Ababneh, P. Schwarz, H. Seidel, U. Schmid, and J. L. Snchez-Rojas, "Quality-factor amplification in piezoelectric mems resonators applying an all-electrical feedback loop," *Journal of Micromechanics and Microengineering*, vol. 21, no. 2, p. 025007, 2011. [Online]. Available: http://stacks.iop.org/0960-1317/21/i=2/a=025007

[65] A. G. Piersol and T. L. Paez, "Harris' Shock and Vibration Handbook: Sixth Edition," *McGraw-Hill*, vol. Ralph E. Blake, Chapter 2: Basic Vibration Theory, pp. 2.18–2.19, 2010.

[66] N. Jackson, R. O'Keeffe, F. Waldron, M. O'Neill, and A. Mathewson, "Evaluation of low-acceleration MEMS piezoelectric energy harvesting devices," *Microsystem Technologies*, vol. 20, pp. 671–680, 2014.

[67] M. Jandak, T. Neuzil, M. Schneider, and U. Schmid, "Investigation on different damping mechanisms on the q factor of mems resonators," *Procedia Engineering*, vol. 168, pp. 929 – 932, 2016, proceedings of the 30th anniversary Eurosensors Conference Eurosensors 2016, 4-7. Sepember 2016, Budapest, Hungary. [Online]. Available: http://www.sciencedirect.com/science/article/pii/S1877705816336219

[68] L. Staaf, E. Khler, M. Soeiro, P. Lundgren, and P. Enoksson, "Smart design selftuning piezoelectric energy harvester intended for gas turbines," *15th International Conference on Micro and Nanotechnology for Power Generation and Energy Conversion Applications (PowerMEMS2015)*, vol. 660, 012125, 2015.

[69] W. Zhou, G. R. Penamalli, and L. Zuo, "An efficient vibration energy harvester with a multi-mode dynamic magnifier," *Smart Materials and Structures*, vol. 21, no. 1, p. 015014, 2012. [Online]. Available: http://stacks.iop.org/0964-1726/21/i=1/a=015014

[70] COMSOL, "COMSOL Multiphysics Reference Manual," *version 5.3*, 2017. [Online]. Available: www.comsol.com

[71] MIDE, "MIDE: Piezoelectric energy harvesters," *Datasheet*, 2013. [Online]. Available: http://www.tande.com.tw/eh-energy-harvesting/Volture_Datasheet_001.pdf

[72] L. G. H. Staaf, P. Lundgren, and P. Enoksson, "Present and future supercapacitor carbon electrode materials for improved energy storage used in intelligent wireless sensor systems," *Nano Energy*, vol. 9, pp. 128–141, 2014.

[73] A. Fujishima and K. Honda, "Electrochemical Photolysis of Water at a Semiconductor Electrode," *Nature*, vol. 238, pp. 37–38, 1972.

[74] P. Simon and Y. Gogotsi, "Materials for electrochemical capacitors," *Nature materials*, vol. 7, 2008.

[75] D. P. Dubal, O. Ayyad, V. Ruiz, and P. Gmez-Romero, "Hybrid energy storage: the merging of battery and supercapacitor chemistries," *Chem. Soc. Rev.*, vol. 44, pp. 1777–1790, 2015.

[76] P. Auerkari, "Thermal energy harvesting from temperature fluctuations," *VTT Manufacturing Technology*, 1996.

[77] D. B. Murray and J. G. Hayes, "Cycle testing of supercapacitors for long-life robust applications," *IEEE Transactions on Power Electronics*, vol. 30, no. 5, pp. 2505–2516, May 2015.

[78] N. R. Council, "Materials for High-Temperature Semiconductor Devices," *The National Academies Press*, 1995.

[79] J. Watson, "Harsh Environmnents Conquered-Low Power, Precision, High Temperature Components for Extreme High Temperature Applications," *Analog Devices Inc.*, vol. MS-2707, 2014.

[80] M. T. Clough, K. Geyer, P. A. Hunt, J. Mertes, and T. Welton, "Thermal decomposition of carboxylate ionic liquids: trends and mechanisms," *Phys. Chem. Chem. Phys.*, vol. 15, pp. 20 480–20 495, 2013.

[81] G. Xiong, A. Kundu, and T. Fisher, "Thermal Effects in supercapacitors," *SpringerBriefs in Thermal Engineering and Applied Science*, 2015.

[82] S. Fendt, S. Padmanabhan, H. W. Blanch, and J. M. Prausnitz, "Viscosities of Acetate or Chloride-Based Ionic Liquids and Some of Their Mixtures with Water or Other Common Solvents," *J. Chem. Eng. Data*, vol. 56, pp. 31–34, 2011.

[83] F. Wendler, L.-N. Todi, and F. Meister, "Thermostability of imidazolium ionic liquids as direct solvents for cellulose," *Thermochimica Acta*, vol. 528, pp. 76 – 84, 2012. [Online]. Available: http://www.sciencedirect.com/science/article/pii/S0040603111005582

[84] R. A. Guidotti and F. W. Reinhardt, "Evaluation of fiber separators for use in thermal batteries," *Sandia Report*, 2006.

[85] Datasheet, "1 Mil Kapton tape, RoHS Compliant," *kaptontape.com*, 2018. [Online]. Available: https://www.kaptontape.com/1_Mil_Kapton_Tapes_Datasheet.php

[86] M. Haque, Q. Li, A. D. Smith, V. Kuzmenko, E. Köhler, P. Lundgren, and P. Enoksson, "Thermal influence on the electrochemical behavior of a supercapacitor containing an ionic liquid electrolyte," *Electrochimica Acta*, 2018. [Online]. Available: http://www.sciencedirect.com/science/article/pii/S0013468618300434

[87] S. Firdosy, B. C.-Y. Li, V. Ravi, J. Sakamoto, T. Caillat, R. C. Ewell, and E. J. Brandon, "Metallization for Yb14MnSb11-Based Thermoelectric Materials," *NASA Tech Briefs*, vol. Aug, p. 13, 2011.

[88] J. Sakamoto, A. Kisor, T. Caillat, L. Lara, V. Ravi, S. Fridosy, and J.-P. Fleuiral, "Mo/Ti Diffusion Bonding for Making Thermoelectric Devices," *NASA Tech Briefs*, vol. July 2007, p. 13, 2007.

References